Geophysical Journal International

Geophys. J. Int. (2020) **221,** 665–682
Advance Access publication 2020 January 16
GJI Seismology

doi: 10.1093/gji/ggaa028

Propagation of distinct Love-wave pulses from regional to teleseismic distances in continental and oceanic environments

Takashi Furumura [1] and Brian L.N. Kennett [2]

[1] *Earthquake Research Institute, The University of Tokyo, 1 Chome-1-1 Yayoi, Bunkyo-ku, Tokyo* 113-0032, *Japan. E-mail: furumura@eri.u-tokyo.ac.jp*
[2] *Research School of Earth Sciences, The Australian National University,* 142 *Mills Rd, Acton, ACT* 0200, *Australia*

Accepted 2020 January 11. Received 2020 January 10; in original form 2019 November 26

SUMMARY

Surface waves are usually dispersive with long wave trains and steady decay of amplitude with distance. However, if the group velocity is nearly constant for a span of periods a strong pulse is produced that retains its amplitude for large distances. This situation arises for the fundamental mode of Love waves in the period band 40–500 s for crust and mantle structures with a positive gradient of *S* wave speed in the uppermost mantle. Such a distinct Love-wave pulse with limited dispersion observed at teleseismic distance is termed the *G* wave in honour of Gutenberg. The long-period *G*-wave pulse caused by large earthquakes carries a large amount of energy to substantial distances, with significant effects across the globe, for example event triggering. A similar G-type Love-wave pulse with a much shorter-period of 10–20 s is generated for crustal structures without thick sediment. Such pulses produce anomalously large ground displacement at near-regional distances with, for example an overestimate of surface wave magnitude. We investigate the generation and propagation mechanism of the G-type Love-wave pulses in the crust and upper-mantle with the analysis of observed strong motion records from the M_w 6.2 2016 Central Tottori earthquake and the M_w 9.0 2011 Off Tohoku earthquake in Japan, in conjunction with 3-D finite-difference simulation of seismic wave propagation and analysis of dispersion curves.

Key words: Numerical modelling; Earthquake ground motions; Surface waves and free oscillations; Wave propagation.

1 INTRODUCTION

The interference of post-critical SH-wave reverberations between the free surface and the increase of seismic wave speed with depth produces Love waves. Usually these surface waves are attenuate gradually since frequency dispersion produces long wave trains.

However, for crust and mantle structures with a steep gradient of *S* wave speed in the uppermost mantle, the dispersion curve of the fundamental-mode Love wave has a nearly constant group velocity of about 4.4 km s^{-1} over a wide period band from 40 to 500 s. The limited dispersion across this wide period band produces a large-amplitude Love-wave pulse that can travel for large distances without significant attenuation.

Such long-period Love-wave pulses were first noticed by Gutenberg & Richter (1934) in teleseismic records, and later named the *G* wave in honour of Gutenberg. The efficient propagation of the *G* wave, especially across oceanic structure, is often recognized in long duration teleseismic records as G1, G2, . . . Gn circling the earth every 2.5 hr. The *G* wave carries substantial energy from large earthquakes and produces significant effects across the globe such as triggered tremors and earthquakes, as reported for the 2011 Off Tohoku, Japan M_w 9.0 earthquake (e.g. Miyazawa 2011; Gonzalez-Huizar *et al.* 2012; Chao *et al.* 2013; Yukutake *et al.* 2013).

For continental paths, without thick sediment, the dispersion curve for fundamental-mode Love waves also has a nearly constant group velocity of about 3.4 km s^{-1} over a wide period band (10–20 s). The very weak dispersion produces a similar G-type Love-wave pulse that can travel a long distance. The propagation of such moderate-period (10–20 s) Love-wave pulses produce large ground motions at relatively large distances. These large ground motions mislead estimates of surface wave magnitude based on distant records. Such magnitude overestimates for the Japan Meteorological Agency value (M_j) relative to moment magnitude (M_w) occur frequently from shallow large earthquakes in western Japan (Furumura and Kennett 2001; Kawamoto 2018). Examples include the 1997 Northern Yamaguchi earthquake (M_j 6.6; M_w 5.9), 2000 Western Tottori, Japan earthquake (M_j 7.3; M_w 6.8), and the 2016 Central Tottori earthquake (M_j 6.6; M_w 6.2). In each case the magnitude overestimate had a large effect on emergency response and assessment of earthquake disaster potential.

The visibility of the two G-type Love-wave pulses of moderate- (10–20 s) and long-period (40–500 s) in the strong motion and

teleseismic broad-band records depends on the magnitude of earthquakes (i.e. source spectrum), propagation distances, and the period range of filtering. The energetic M_w 9.0 source of the 2011 Off Tohoku, Japan earthquake was able to produce both G-pulses clearly in near-regional broad-band records. Such G-type pulses occur only for Love waves and not for Rayleigh waves, though a weak Airy phase can cause some amplification of the long Rayleigh wavetrain.

In this study, we investigate the cause of such distinctive G-type Love-wave pulses for the moderate- (10–20 s) and long-period (40–500 s) bands and their capacity to carry large amounts of energy from large earthquake sources to regional and teleseismic distances. We analyse strong motion records for the Central Tottori, Japan earthquake (M_w 6.2; 8 km depth) of 21 October 2016, and regional to teleseismic records for the Off Tohoku, Japan earthquake (M_w 9.0; 23 km depth) of 11 March 2011. To complement the observations, and to seek further insights into the understanding of the generation and propagation mechanism of the G-type Love-wave pulses, we conduct numerical simulation of seismic wave propagation in heterogenous crust and upper-mantle structures. We use 3-D finite-difference method (FDM) simulation with a heterogeneous crust and mantle models, and theoretical dispersion curves. The simulation results reproduce the observed Love-wave pulses at regional to teleseismic distances quite well, and so aid the analysis and interpretation of observed Love-wave pulses. In addition, the snapshots and movies obtained by the simulation demonstrate the generation of the G-type pulses and their interaction with crust and upper-mantle structure.

The moderate- and long-period G-type pulses are similar phenomena linked to the increase in seismic wave speeds in the crust and mantle structure with depth. Their propagation characteristics are depend strongly on structure, particularly sediment and crustal thickness.

2 MEDIUM-PERIOD LOVE-WAVE PULSES AT NEAR-REGIONAL DISTANCES

2.1 Ground motions from 2016 Central Tottori earthquake

In southwest Japan, shallow strike-slip earthquakes occur in a stress field with east–west compression due to the collision of the Philippine-sea and the Pacific Plate with the continental plate. The Central Tottori, Japan, M_w 6.2 earthquake of 21 October 2016 at a depth of 8 km is typical for the tectonic environment of southwest Japan.

Fig. 1(a) presents the distribution of peak ground horizontal displacement (PGD) extracted from the strong motion records of 595 K-NET and KiK-net stations of the National Research Institute for Earth Science and Disaster Resilience (NIED 2019a) after integrating acceleration to displacement. Large ground motion, 0.2–5 cm, spreads from the epicentre in Tottori to the southwest towards Kyushu and to the northeast towards central Japan and extends to epicentral distances beyond 400 km. The pattern of PGD corresponds to the four-lobed Love-wave radiation pattern of this strike-slip focal mechanism of this earthquake. However, the large ground motion is only partially recorded in the K-NET and KiK-net stations on land. Similar patterns of enhanced PGD were also found for other large earthquakes in western Japan, for example the 2000 Western Tottori earthquake (M_w 6.8; 8 km depth), 2005 Western Fukuoka earthquake in (M_w 6.7; 9 km depth) and 2016 Kumamoto earthquake (M_w 7.0; 12 km depth). Results for these events are shown in Fig. S1.

Figs 1(b) and (c) show record sections of transverse (T) and radial (R) component ground displacement from F-net broad-band stations of NIED (NIED 2019b). A bandpass filter (0.01–1 Hz) is applied to the records and they are then integrated from velocity to displacement. The strongest ground motion occurs on section *a–a'* from the hypocentre to Kyushu. A large-amplitude Love-wave pulse with a dominant period of about 15 s, and velocity around 3.4 km s^{-1} is the most prominent feature of the T-component record section for western Japan. The observed Rayleigh wave on the R component is very weak, less than one quarter of the Love wave amplitude, due to weaker radiation of the Rayleigh wave in this direction from the strike-slip earthquake source (see, Fig. 1a for radiation pattern). Note that the amplitude of the R-component record in Fig. 1(c) is multiplied by 2 to enhance weak signals.

Thus, the anomalous spread of larger PGD in western Japan is generated by the propagation of Love-wave pulses with periods around 15 s. As the Love wave travels through west Kyushu, about 500 km from the epicentre, it attenuates gradually due to dispersion after traversing a large sedimentary basin. The Rayleigh waves in western Japan show much stronger dispersion and so do not produce pulse-like arrivals.

In contrast to western Japan, in propagation from central Japan to the northeast we do not see pulse-like arrivals at larger distances due to the dispersion and attenuation of Love waves. The large difference in the character of the Love wave propagation in these two directions is demonstrated in Fig. 2 with 3-component records and the frequency-time plots for observations at stations STMF in Kyushu (471 km distance) and at KZKF (469 km distance) in central Japan. A clear Love-wave pulse is recorded at STMF with a maximum ground amplitude of 0.25 cm, and the frequency–time plot indicates that this is formed by a large signal with a wide period band (10–20 s). Whereas, at KZKF the Love waves show significant dispersion for periods between 10 and 40 s producing a long wavetrain with a duration of more than 100 s. The differences between the Love-wave propagation to Kyushu and to central Japan are associated with structure rather than the source, since the strength of the Love-wave radiation is almost the same in the two directions.

2.2 Dispersion curves

We can shed light on the nature of the differences in propagation characteristics for medium period waves with the aid of theoretical dispersion curves. We use the velocity structure in western and central Japan from the Japan Integrated Velocity Structure Model (JIVSM; Koketsu *et al.* 2008). Fig. 3(a) shows the thickness of sedimentary layer in the area around Japan from JIVSM, and Fig. 3(b) demonstrates crustal thickness. There is a thick sediment cover (Vs = 0.55–2.0 km s^{-1}) over rigid bedrock (Vs > 3.0 km s^{-1}) in central to northern Japan. The thickest sediments (3–8 km) occur near Niigata and in Hokkaido. Sediments are generally thin in the area around Tottori of western Japan and basement outcrops widely. Fig. 3(b) shows the thickness of the crust, there is thicker crust (30–35 km) along the spine of the Japanese archipelago, but it thins gradually (<20 km) toward the surrounding sea.

Figs 4(a) and (b) display theoretical dispersion curves for the fundamental and first and second higher-modes of Love and Rayleigh waves calculated by using 1-D velocity structures (Fig. 3c), together with the measured group velocities of the Love wave (open

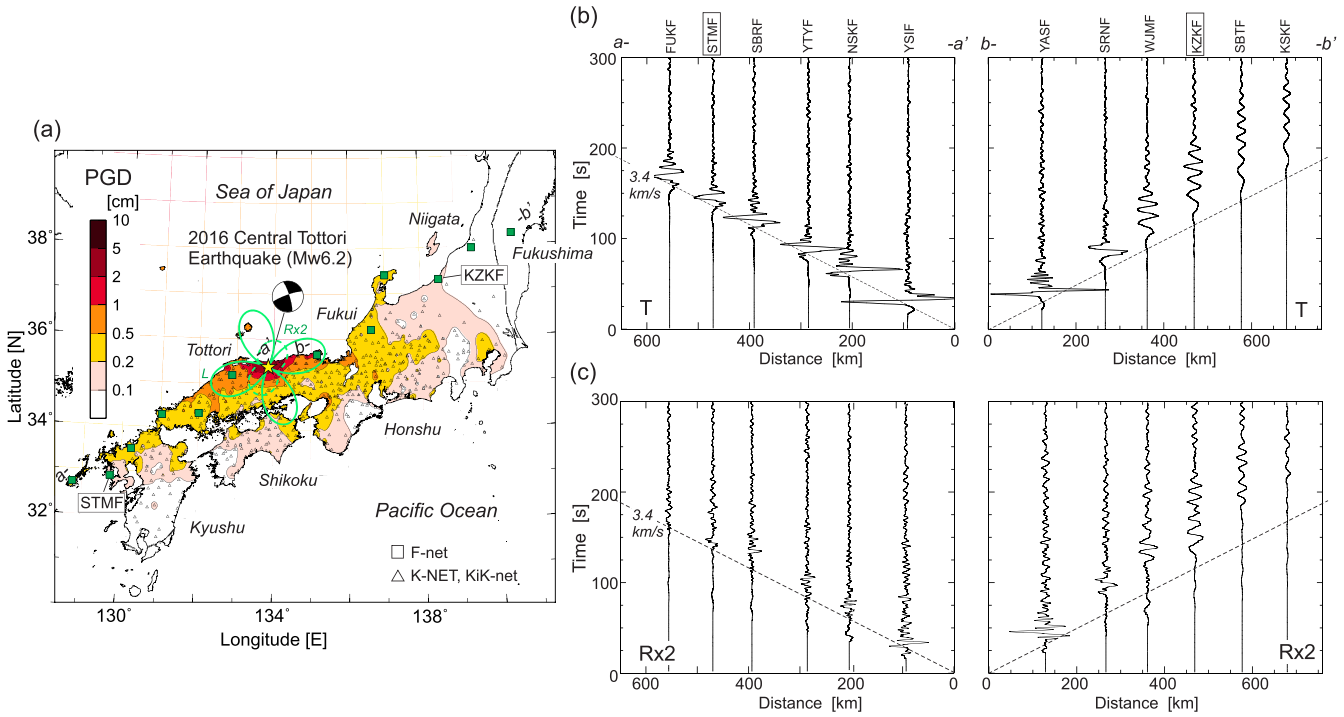

Figure 1. (a) Peak ground displacement (PGD) for the 2016 Central Tottori, Japan, M_w 6.2 earthquake, extracted from strong motion records of the K-NET and KiK-net (triangle marks). The radiation pattern of Love (solid line) and Rayleigh wave (dashed line) in period of 10 s are shown, with a CMT focal mechanism of the F-net. (b) Record sections of transverse (T) and (c) radial (R) component ground displacement for F-net broad-band stations for paths to Kyushu *(a–a')* and to Fukushima (*b–b'*) (green squares in the PGD map). A bandpass filter was applied for the band 0.01–1 Hz. The group velocity of 3.4 km s^{-1} is indicated. The amplitude of the R in record section and radiation pattern are doubled to enhance visibility.

circles) from the frequency–time plots (Fig. 2). The velocity models are taken from JIVSM at the midpoint A between the epicentre in Tottori to Kyushu (*a–a'* of Fig. 1) and the location B midway to Niigata (*b–b'*) (see, Fig. 3 for locations). The eigenfunctions of the fundamental-mode Love wave calculated for each model are shown in Figs 4(c) and (d), as a function of period from 5 to 40 s showing the sensitivity to structure.

The theoretical dispersion curve of the fundamental-mode Love wave calculated for the western Japan model (Fig. 4a) shows a nearly constant group velocity ($u = 3.2$ km s^{-1}) in periods between 7 and 20 s, which explains the origin of the large-amplitude observed Love-wave pulses in western Japan. The group velocities measured from the frequency–time plot (Fig. 2a) also display a flat group velocity in this period band, but the velocities are slightly faster than the theoretical values obtained with the 1-D velocity model. The constant group velocity is accompanied by a linear increase in phase velocity c (from 3.3 to 3.8 km s^{-1}) in this period band. As can be seen from the behaviour of the fundamental Love wave eigenfunctions, the lower cut-off period (7 s) for the Love-wave pulse is determined by the thickness and wavespeed of the sedimentary layer at the surface, and the upper cut-off period (20 s) is controlled by the crust and upper-most mantle structure.

In contrast, the theoretical dispersion curves for the central Japan 1-D velocity model at location B (Fig. 4b) and measured group velocities show strong dispersion of the fundamental-mode Love wave in period 7–20 s as we saw in the record section along *b–b'* in Fig. 1(b) due to a thick sedimentary cover (>3 km, Fig. 3a). With the presence of thick sedimentary layer, the eigenfunctions of the fundamental-mode Love wave at shorter wavelengths are much more sensitive to the shallower structure (Fig. 4d) than those at location A (Fig. 4c). This dispersion produces a steady increase in group velocity with period from 7 to 50 s, and so explains the long dispersed Love wavetrains observed in central Japan (Fig. 1b).

Rayleigh wave dispersion in western Japan shows a mild group velocity minimum of about 2.8 km s^{-1} at period around 17 s (Fig. 4a) that produces some amplification, as well as significant dispersion. For central Japan there is strong dispersion with frequency (Fig. 4b).

We note that the theoretical dispersion curves for western Japan (Fig. 4a) also predict another possible surface wave pulse associated with higher-modes with nearly constant group velocity of about 4.4 km s^{-1} in the period band between about 20 and 40 s. However, these higher-mode Love and Rayleigh wave pulses are not visible in the observed record section, probably because they are much smaller in amplitude than the fundamental mode surface wave for the shallow source and there is weak radiation of longer-period (20–40 s) signals from the moderate-scale (M_w 6.2) earthquake source.

2.3 3-D FDM simulation

With the insight gained from the dispersion analysis, we examine the generation and propagation process of the distinctive Love-wave pulse in western Japan during the 2016 Central Tottori, Japan, M_w 6.2 earthquake, using a 3-D FDM simulation of seismic wave propagation based on the OpenSWPC code (Maeda *et al.* 2017) suitable for large-scale modelling using parallel supercomputers. We use a heterogeneous crust and upper-mantle structure of the JIVSM (Koketsu *et al.* 2008).

The area of the 3-D FDM simulation is 600 km by 1368 km in the parallel and normal directions for the focal mechanism of this earthquake (Fig. 5), and 120 km in the vertical direction. The domain is discretised with a grid interval of 0.25 km. The JIVSM

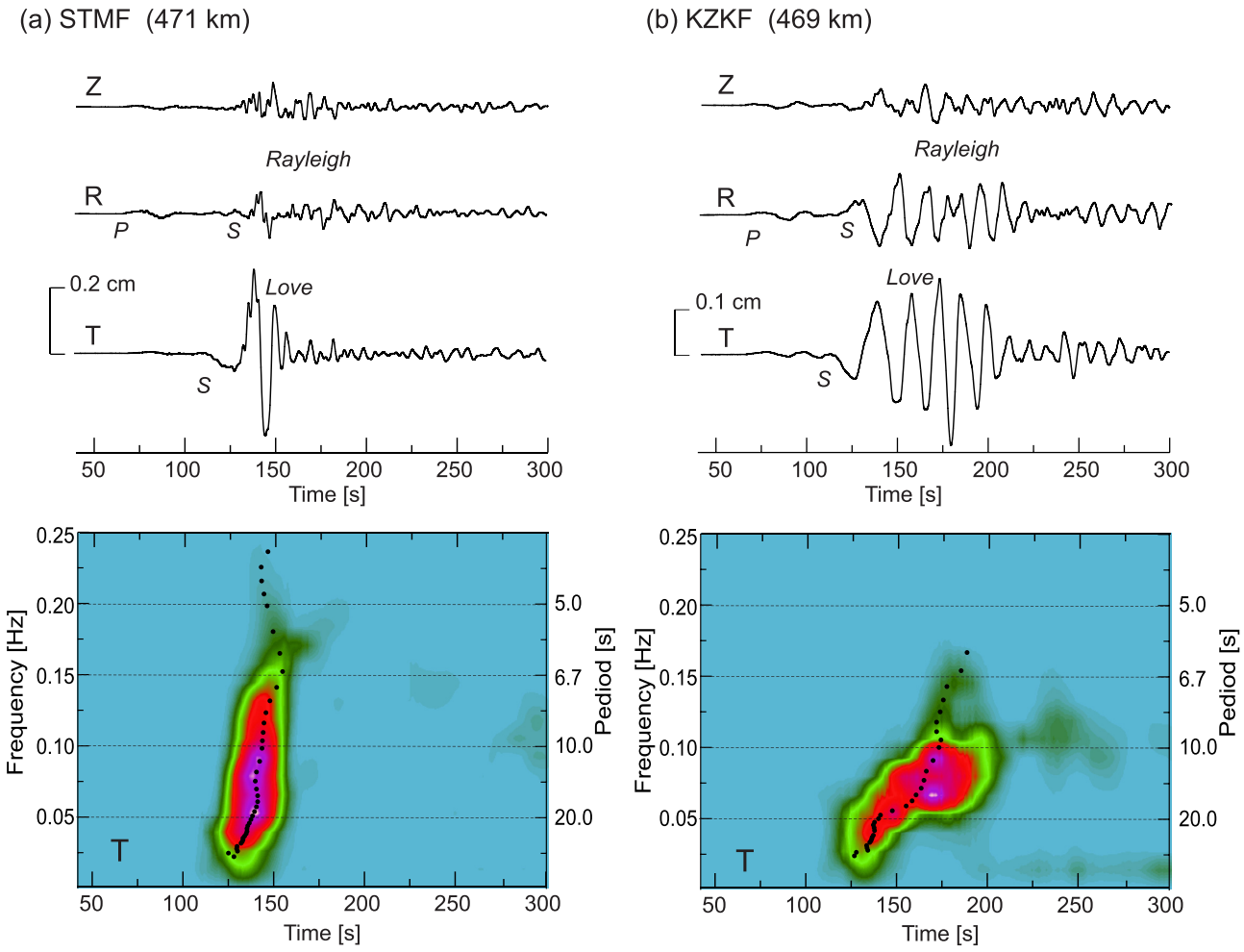

Figure 2. Three-component displacement records for the 2016 Central Tottori, M_w 6.2 earthquake. Vertical (Z), radial (R) and transverse (T) motions recorded at F-net stations are displayed (see, Fig. 1 for locations). (a) STMF to the southwest at epicentral distance 471 km and (b) KZKF to the northeast at 469 km. The lower panels present frequency–time plots for the T-component record at each station with measured group velocity at each frequency.

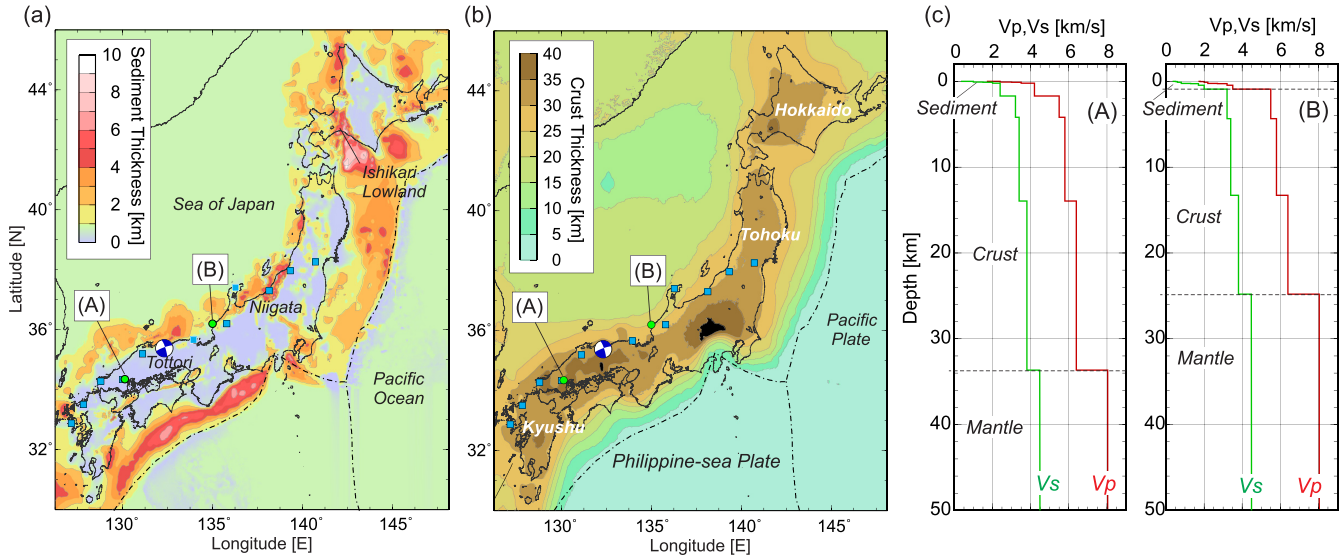

Figure 3. (a) Map showing the depth of the thickness of sedimentary layer ($Vs = 0.55$–2.0 km s^{-1} layer) and (b) the crustal thickness from the JIVSM model (Koketsu *et al.* 2008). (c) 1-D velocity profile at locations A and B (green circles in Figs 3a and b). Blue squares denotes the F-net stations used for record sections in Fig. 1.

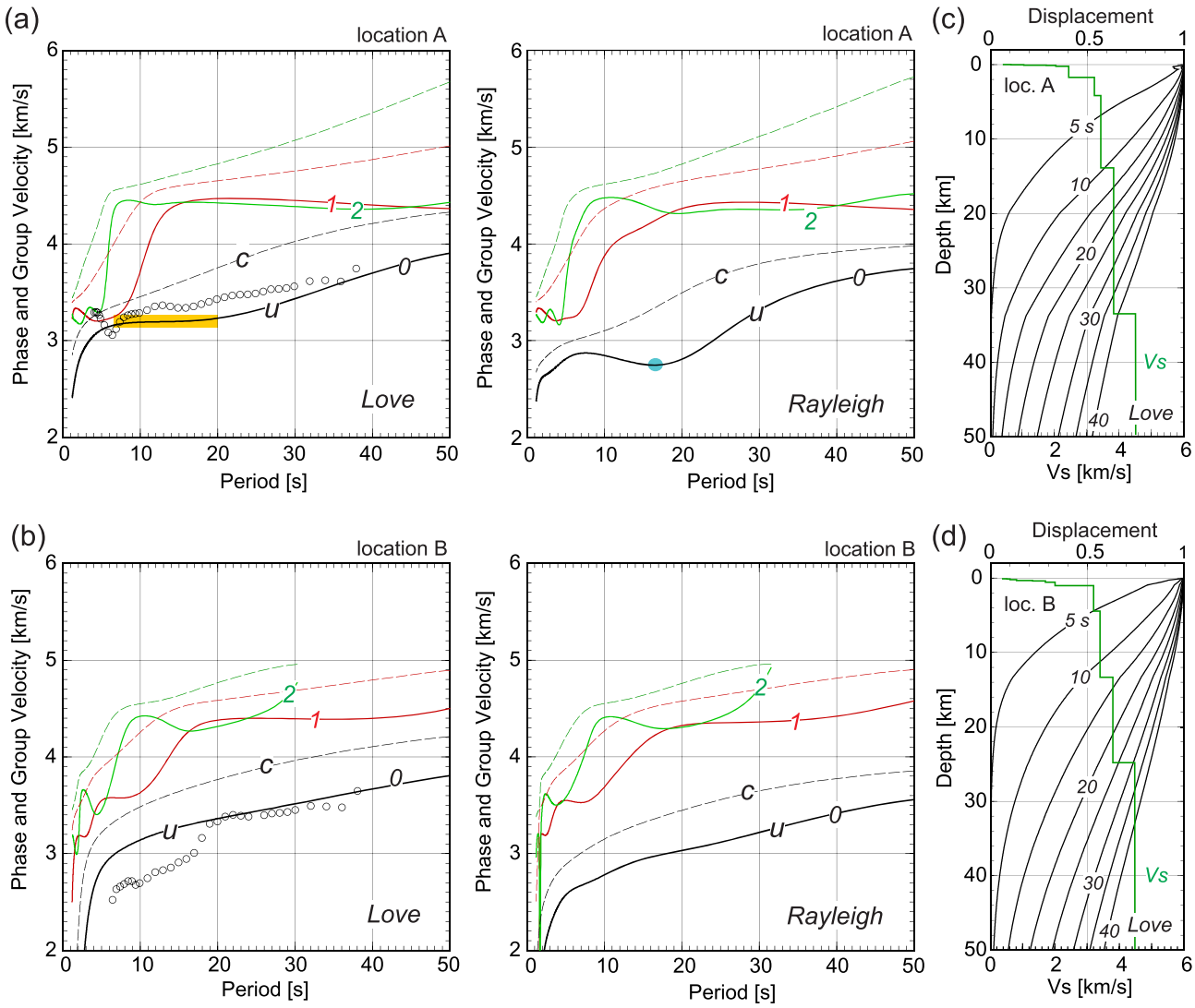

Figure 4. (a) The theoretical dispersion curves for group velocity (u; solid lines) and phase velocity (c; dashed lines) for the fundamental (black), first (red) and second (green) higher-modes of Love and Rayleigh waves using the JIVSM model for western Japan (location A, see, Fig. 3) and (b) for central Japan (location B). The open circles denote the measured group velocity of the Love wave (see, Fig. 2). Yellow highlight indicates nearly flat group velocity in the theoretical dispersion curve that corresponds to a Love-wave pulse, and the blue circle indicates the Airy phase (minimum group velocity) of Rayleigh wave. (c) Eigenfunction of the fundamental-mode Love wave as a function of period (5, 10, . . . , 40 s) and *S*-wave velocity (green line) at locations A and (d) at location B. The amplitude is normalized to the displacement at the surface.

structure consists of sedimentary layers (Vs = 0.55–2.0 km s^{-1}) on top of basement rocks in the upper crust (Vs = 3.2 km s^{-1}), middle crust (Vs = 3.4 km s^{-1}), and lower crust (Vs = 3.8 km s^{-1}). The velocity and density structure below Moho is based on the *ak135* reference earth model (Kennett *et al.* 1995), and anelastic attenuation (Qp and Qs) is taken from *ak135-f* (Montagner & Kennett 1996). The subducting Pacific and Philippine-sea plates beneath central to western Japan are modelled based on the JIVSM, however such deep structure will not have a large effect on the propagation of the fundamental-mode surface waves for periods of 10–20 s.

The source of the 2016 Central Tottori earthquake was represented by a double-couple point-source from the F-net CMT focal mechanism (strike = 342°, dip = 80° and rake = 9°) placed at a depth of 8 km. The M_w 6.2 earthquake source is represented by a triangular source–time function with a duration of 7 s, which results in a flat displacement spectrum on the period longer than the corner period (7 s). In this simulation, the propagation of seismic waves for periods longer than 2.3 s can be examined accurately with a sampling of 5 FDM gridpoints per minimum wavelength of *S* wave.

Fig. 6 presents the result of the simulation of wave propagation from the 2016 Central Tottori earthquake, with a record section of seismograms along profiles *a–a'* in Fig. 5 along with snapshots of the T-component velocity wavefield at 20, 60, 110 and 160 s from the earthquake origin time (also see Movie S1 in the Supporting Information). The same bandpass filter between 0.01 and 1 Hz is applied to both synthetic and observed seismograms. The snapshots from the 3-D FDM simulation display velocity, rather than displacement, so short-period components are enhanced compared to the displacement record sections.

The first arrival is a *Sn* wave travelling just below the Moho with a mantle *S*-wave speed of about 4.2 km s^{-1}, which is followed by a large-amplitude Love-wave travelling horizontally along

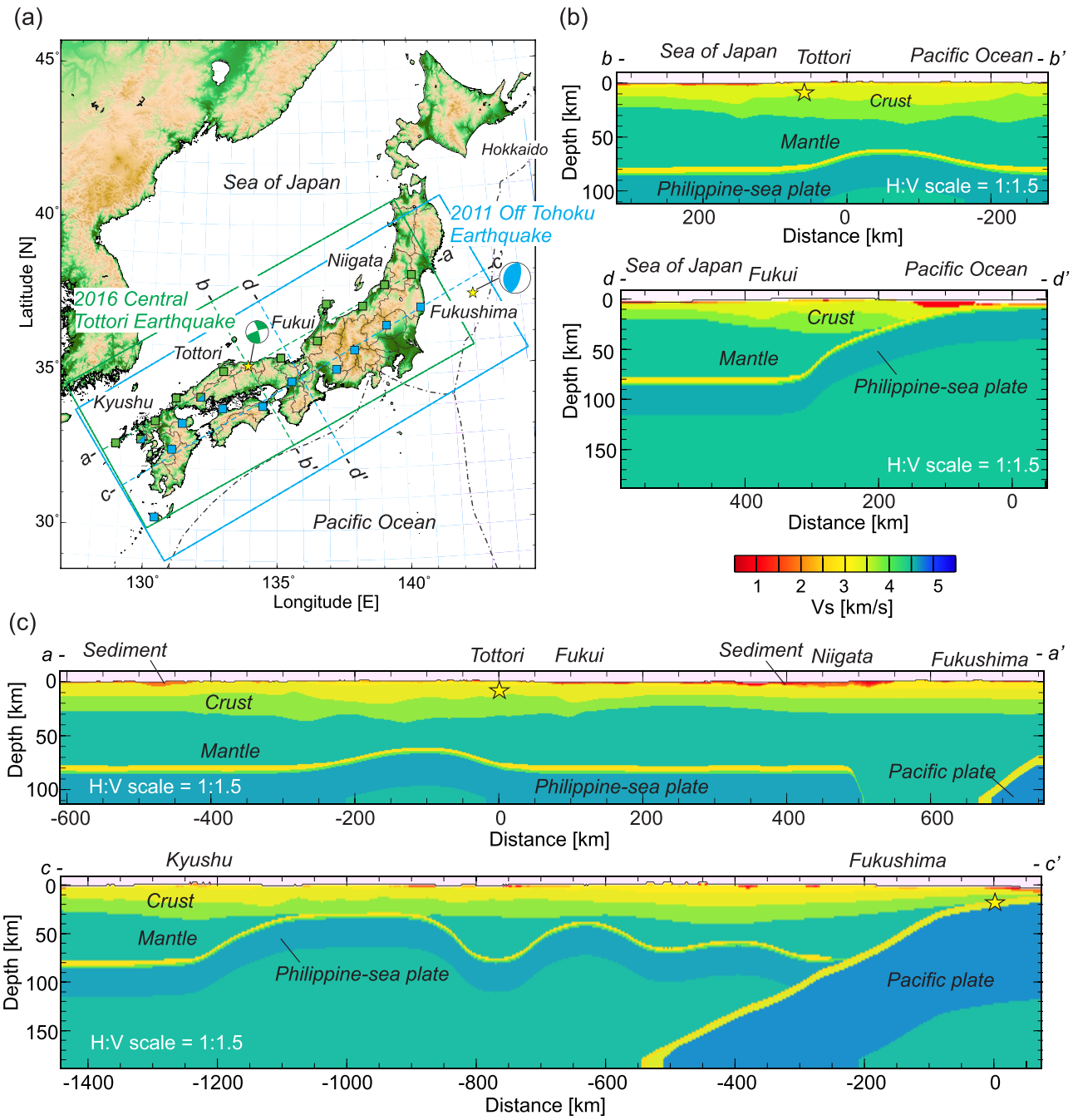

Figure 5. (a) Area used for the 3-D FDM simulation of seismic wave propagation for the 2016 Central Tottori earthquake (green rectangle) and the 2011 Off Tohoku earthquake (blue rectangle) with the location of F-net stations (green and blue squares). (b) Vertical cross section of *S*-wave velocity (*Vs*) structure along lines *b–b'* and *d–d'*, and (c) *a–a'* and *c–c'* of the FDM model exploiting the JIVSM model (Koketsu *et al.* 2008).

the surface, with a large compact wave packet. The rapid decay of amplitude from surface to the deeper crust represents the fundamental-mode Love wave, accompanying a weakly dispersed short-wavelength Love wave travelling in the upper crust (see, 60 and 110 s snapshots). For earlier times after the earthquake, the snapshots show a symmetrical pattern of Love-wave propagation from the source in both directions. The propagation of the Love-wave pulse is very clear in western Japan, maintaining a compact wave packet to over 400 km from the epicentre. Then, some elongation of the Love-wave pulses by dispersion occurs as they traverse thick sediments in Kyushu (160 s snapshot). However, for propagation through central Japan the originally short Love-wave pulses gradually spread with distance. The dispersion of the Love-wave pulses become more pronounced in northern Japan where thick (>1–4 km) sediments are present between 200 and 500 km from the source (110 and 160 s snapshots).

The simulated T-component record section of displacement motion shown in Fig. 6(a), explains the observed ground motions at the F-net stations (blue traces) fairly well, indicating the effectiveness of the JIVSM and a point double-couple source representation of the M_w 6.2 earthquake for modelling of surface waves with dominant period around 10–20 s. However, some overestimates of

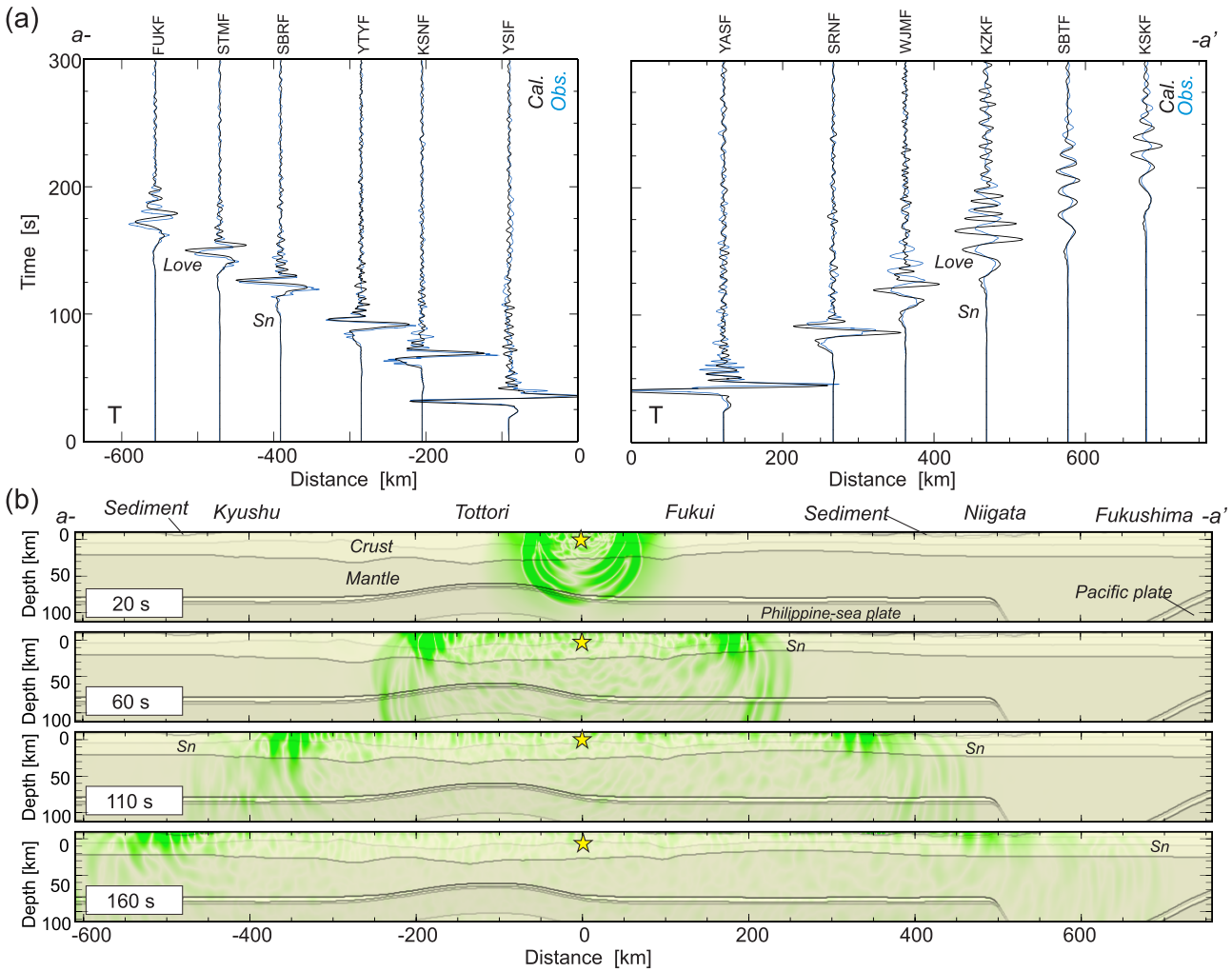

Figure 6. (a) Calculated record section of the T-component of ground displacement at F-net stations (see Figs 1 and 5 by green squares) obtained from the 3-D FDM simulation, compared with the observed ground displacement (blue traces). A bandpass filter between 0.01 and 1 Hz is applied to both observed and calculated waveforms. (b) Snapshots of seismic wavefield of T-component velocity at 20, 60, 110 and 160 s after the earthquake origin time in vertical cross section of *a–a'* in Fig. 5 (see also Movie S1).

amplitude and phase delay in the simulation results relative to the observed ground motions for stations KZKF and KSKF indicate the need for mild model refinement in the shallow structure near the stations. Nevertheless, the result of the 3-D FDM simulation well reproduces the characteristics of the distinctive Love-wave pulse in western Japan from a shallow large earthquake, with maintenance of a large-amplitude pulse for more than 500 km. The simulation also explains the attenuation and elongation of the Love wave towards central to northern Japan after traversing thick sedimentary layers beneath the Sea of Japan and in Niigata, confirming the dispersion analysis (Fig. 4).

3 LONG-PERIOD LOVE-WAVE PULSES AT REGIONAL DISTANCES

3.1 Ground motions from the 2011 Off Tohoku earthquake

We have demonstrated a distinct Love-wave pulse with a dominant period of about 15 s travelling in western Japan caused by the shallow, M_w 6.2, earthquake source of the 2016 Central Tottori earthquake.

The much more energetic source of the Off Tohoku, Japan, M_w 9.0 earthquake of 11 March 2011 (depth 20 km) produced much longer period (70 s) Love-wave pulses travelling across central to western Japan. These pulses produced large ground motions over 1000 km from the epicentre.

Fig. 7(a) shows the PGD of horizontal ground motions obtained from 1236 K-NET and KiK-net records, demonstrating the broad spread of the area of large ground motion (>10 cm) over the Pacific Ocean side from Tohoku to the Kanto region around Tokyo, parallel to the source-rupture area of this earthquake of about 500 km by 200 km. This shallow-angle reverse-fault earthquake produced destructive Love waves to the north towards Hokkaido and to the southwest through central to western Japan. A large Rayleigh wave was radiated to the northwest direction towards Tohoku.

Figs 7(b) and (c) show the record sections of T- and R-component ground displacements at F-net stations from the epicentre to Kyushu and to Hokkaido (see, Fig. 6a for locations), along the directions where Love waves are enhanced. Love waves build from the interference of SH-wave reflections in the lower wave speeds near

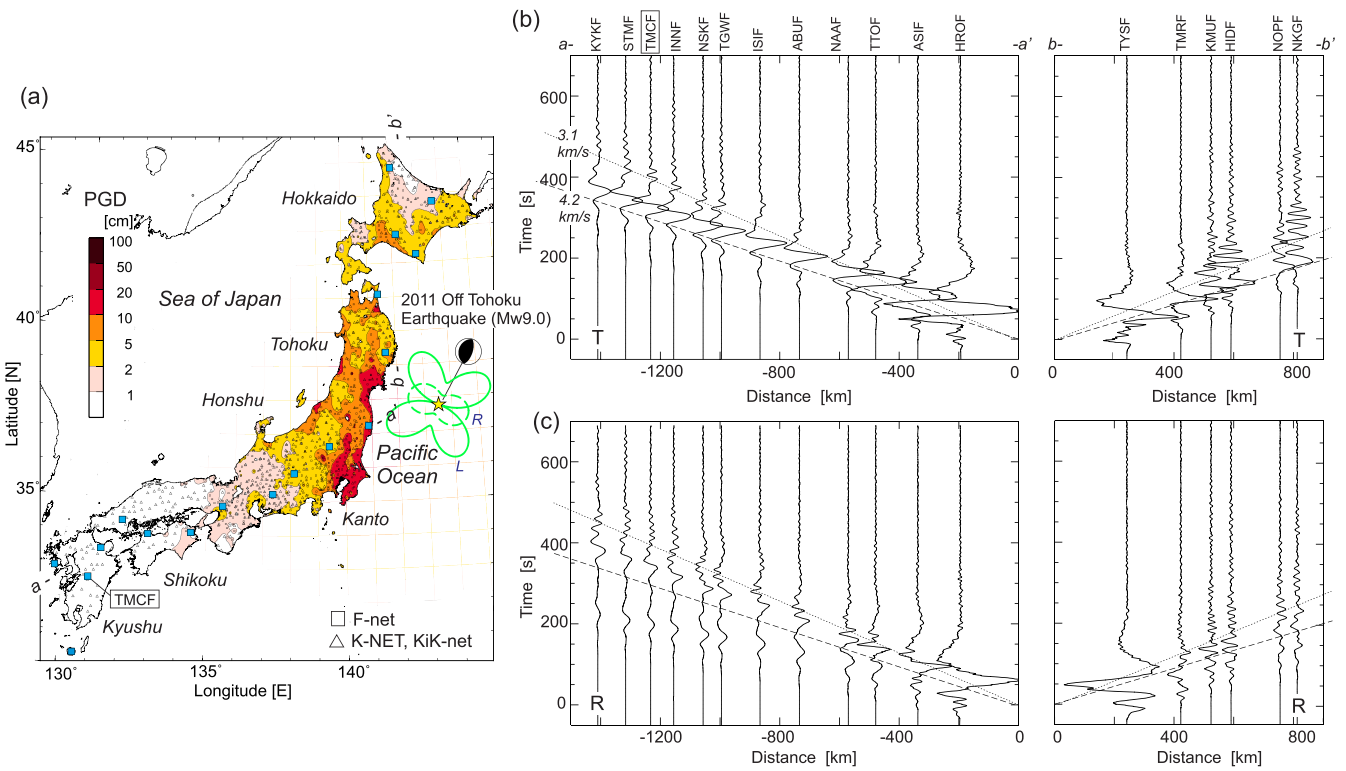

Figure 7. (a) Peak ground displacement (PGD) caused by the 2011 Off Tohoku, Japan, M_w 9.0 earthquake, from the strong motion records of the K-NET and KiK-net stations (small triangles). The radiation pattern of Love wave (solid line) and Rayleigh wave (dashed line) for 40 s period are shown with the GCMT focal mechanism. (b) Record section of T- and (c) R-component ground displacement from F-net stations from source towards Kyushu (*a–a'*; blue squares in the PGD map) and towards Hokkaido (*b–b'*). A bandpass filter between 0.005 and 1 Hz is applied. Group velocities 4.2 and 3.1 km s^{-1} are indicated on the record section.

the surface. For 70 s period the Love waves emerge as a distinct feature at around 500 km from the epicentre. The observed records show Love-wave pulses with a dominant period of about 70 s, with weak dispersion for longer periods from 100–20 s. The propagation speed of the longer-period 70 s Love-wave pulse in western Japan from the Off Tohuku event is about 4.2 km s^{-1}, which is much faster than the 3.4 km s^{-1} velocity of the.15 s Love-wave pulse seen in western Japan during the M_w 6.2 Central Tottori earthquake (Fig. 1).

Following the fast 70 s period Love-wave pulse in western Japan, we also see a 20 s Love-wave pulse, similar to the 15 s pulse for the 2016 Central Tottori earthquake. The slightly longer dominant period of this Love-wave pulse from the Off Tohoku event is likely to be due to the attenuation of short-period components after longer distance propagation. The separation of the 70 s and the later 20 s Love-wave pulses becomes clearer at larger distances since they propagate at different speeds. Fig. 8 shows three-component displacement record at the station TMCF in Kyushu for epicentral distance of 1232 km, and a frequency-time plot of the T-component motion. The long- and moderate-period Love-wave pulses are composed of large signals with period range from about 20 to 100 s and 13 to 20 s.

These two Love-wave pulses in the moderate- and long-period bands were not produced by the foreshock (M_w 6.0) of the Off Tohoku earthquake, which generated only the shorter-period component (see Fig. S2) since this smaller magnitude source did not radiate significant long-period components (>20 s). The long-period (70 s) Love-wave pulse can only be generated in the case of large ($M > 8$) earthquakes, because of the corner period associated with the earthquake source.

In contrast to the clear propagation of the Love-wave pulses in central-western Japan, the record section of wave propagation to Hokkaido shows strongly dispersed Love waves even for the long-period components. Such strong dispersion and elongation of Love-wave trains in the long-period components arises from traversing very thick (>5 km) sediments extending from the Pacific Ocean to the Ishikari lowlands of Hokkaido (Noguchi *et al.* 2017, also see Fig. 3a for sedimentary thickness). Rayleigh waves have large amplitude in Tohoku where radiation is favourable. However, to central-west Japan and to Hokkaido, the radiation of the Rayleigh wave is weak and the dispersion is stronger, causing a dramatic decrease in the amplitude with propagation distance.

3.2 Dispersion curves

The generation of the two Love-wave pulses in the moderate- and long-period bands at regional distance can be confirmed from the theoretical dispersion curve of fundamental-mode Love wave shown in Fig. 9(a). The model shown in Fig. 9(e) is based on the *ak135* reference earth model (Kennett *et al.* 1995) with the sedimentary layers in western Japan from JIVSM (Koketsu *et al.* 2008) in the near surface (Figs 3c-A).

In order to investigate the dispersion properties of the Love and Rayleigh waves generated by large earthquakes in a wide period band, the horizontal axis of the dispersion diagram has been expanded to much longer period (1000 s) and displayed on a logarithmic scale (Figs 9a–c). Also we plot the group velocities of the Love wave travelling to Kyushu, extracted from the frequency-time

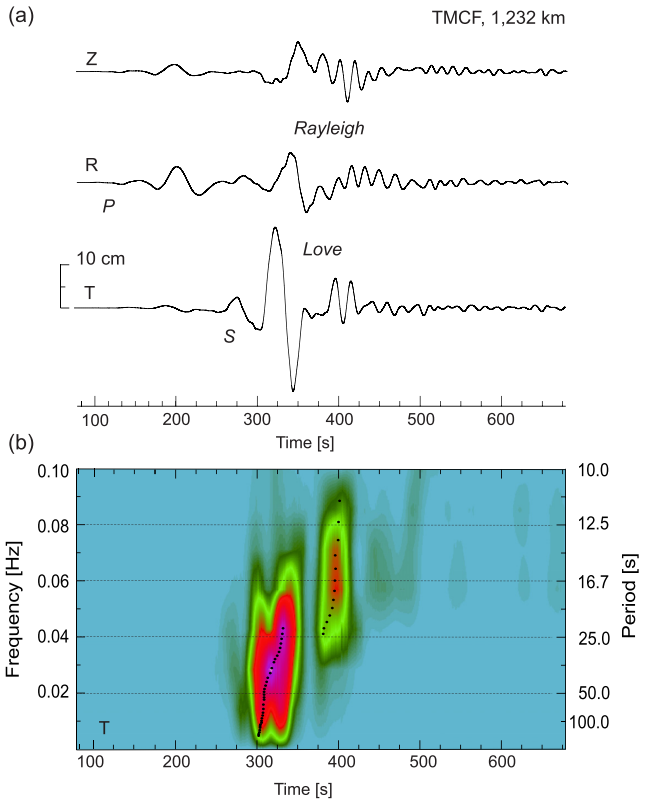

Figure 8. (a) Three-component ground displacement record for the 2011 Off Tohoku, Japan, M_w 9.0 earthquake at station TMCF in Kyushu at an epicentral distance of 1232 km (see, Fig. 7a for location). (b) Frequency–time plot of the T-component ground motion and black dotes denote measured group velocity of Love wave.

plot shown in Fig. 8(b). The calculated fundamental-mode Love-wave dispersion curve shows two set of flat group velocity benches around 3.3 and 4.3 km s^{-1} for the period bands 7–20 s and 80–300 s. These features correspond well to the observed moderate- and longer-period Love-wave pulses in the record section of the 2011 Off Tohoku earthquake and the frequency-time plot of the observed waveform (Figs 7 and 8). The observed group velocity of the Love wave at station TMCF also shows two set of flat group velocity benches for the period bands 6–20 s and 40–180 s, though they are about 0.1–0.2 km s^{-1} slower than the theoretical dispersion curve due to deviation in velocity structure in western Japan from the *ak135* model, notably a slower upper mantle.

As noted above, the first flat group velocity bench of the fundamental-mode Love wave in the moderate-period (7–20 s) band is generated by crust covered with a low-velocity sedimentary layer (Fig. 9a). Similarly, the second flat group velocity bench in the longer-period (80–300 s) band is generated by the low-velocity crust above the upper-mantle structure. Such sensitivity of the Love-wave character as a function of depth can be confirmed from the nature of the eigenfunctions of the fundamental-mode Love wave for moderate and longer periods (Fig. 9d). In the case of a much thicker 55 km crustal structure, the flat group velocity of the fundamental-mode Love wave occurs in a narrower period band (150–240 s) with a slower wave speed (4.2 km s^{-1}) (Fig. 9b). Thus, the long-period Love-wave pulse is likely to occur for ordinary continental crust (about 35 km) rather than thick (55 km) crust.

The generation of the long-period Love-wave pulse is also strengthened by increasing *S*-wave velocity with depth in the upper-mantle structure (Sato 1958). The theoretical dispersion curve calculated by the modified *ak135* model with sediments layer but excluding the velocity gradient of the upper-mantle structure does not show a flat group velocity bench, but instead shows a velocity increase with period (Fig. 9c). The distinctive Love-wave pulse in two period bands is thus a universal phenomenon caused by the general velocity structure of the crust with a thin sedimentary layer and gradients in the upper mantle.

For reference, we have calculated the theoretical Rayleigh-wave dispersion curves for each model and examined the group velocities in period band between 2 and 800 s. These results confirm that the Rayleigh wave does not generate a pulse-type wave, though weak Airy phases for periods around 18 and 200 s can help to amplify some parts of the Rayleigh wavetrain but cannot produce pulse-like signals (Figs. 9a-c).

3.3 3-D FDM simulation

To confirm the propagation process of two Love-wave pulses of moderate (20 s) and longer (70 s) periods in western Japan, with interaction of crust and upper-mantle structure, we have made a 3-D FDM simulation of seismic wave propagation from the 2011 Off Tohoku earthquake using the JIVSM model. The area of this simulation is 640 km by 1536 km in the horizontal directions and 200 km in depth, discretised with a grid interval of 0.25 km (Fig. 5). The source model of the earthquake was represented by a point double-couple source with the GCMT focal mechanism (strike = 203°, dip = 20°, rake = 88° depth = 20 km) and 55 s triangular source time function. Such a point-source approximation of a large earthquake is only valid at large distances.

Fig. 10 presents the result of this 3-D FDM simulation with snapshots of the T-component wavefield in a vertical cross section (*c*–*c'* in Fig. 5) at 30, 120, 210, 300 and 390 s from the CMT origin time. A synthetic record section of T-component ground displacement at the F-net stations (black traces, see, Fig. 7a for locations) is compared with the observed record at the F-net stations (blue traces). Despite the simulation using a simplified point-source model, a fairly good match between simulated and observed Love waveforms confirms the effectiveness of the present simulation for modelling long-period Love waves, though there are differences in travel time and amplitude at short distances.

The snapshots show that the long-period Love-wave pulse penetrates into the upper-mantle to depth of more than 100 km. These waves propagate horizontally in the crust and upper-mantle with a speed of about 4.4 km s^{-1} (see, 120 s snapshot). Following this long period pulse, a weakly dispersed moderate-period (20 s) Love-wave pulse confined to the upper crust can be seen, travelling at about 3.1 km s^{-1} (210, 300 and 390 s snapshots). Although the 70 s period Love-wave pulse with longer wavelength can propagate over large distances across the sedimentary basin in Kyushu, the 20 s Love-wave pulse is dispersed and attenuates rapidly after passing through the thick sedimentary layer (390 s snapshot).

The T-component record section shows the 20 s Love-wave pulse travels to Kyushu, more than 1300 km from the epicentre, gradually separating from the preceding long-period (70 s) Love wave pulse of higher wave speed (4.2 km s^{-1}). The linear trend of arrival times does not point to the origin time of the record section, indicating that this 20 s signal was radiated at different place from the CMT source location and at later time. This late generation is consistent with

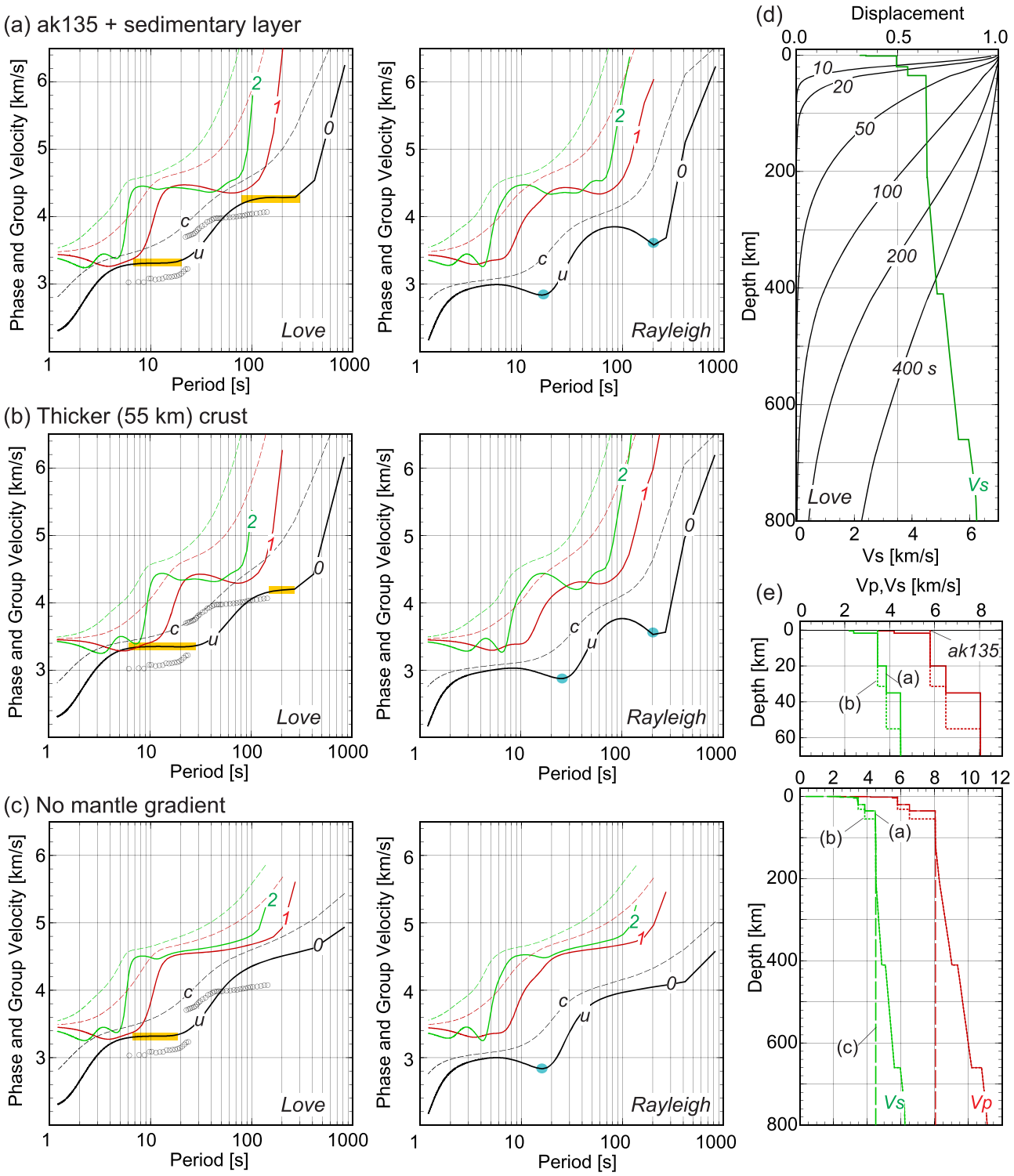

Figure 9. Theoretical dispersion curves of the fundamental mode (black) and first (green) and second (red) higher-modes of Love and Rayleigh wave group (u) and phase (c) velocities obtained by (a) *ak135* reference earth model (Kennett *et al.* 1995) with low-velocity sedimentary layer at the top [see, velocity profile of (e)], (b) modified model for a thicker 55-km-thick crust, (c) the model without velocity gradient in the upper-mantle [see, profile (e)]. Yellow highlights indicate zone of nearly flat group velocity in the fundamental-model Love wave dispersion which corresponds to Love-wave pulse. Blue circles denotes the Airy phase with a minimum group velocity. (d) Eigenfunction of fundamental-mode Love wave for each period and *S*-wave velocity structure. The amplitude is normalized to the displacement at the surface. (e) *P*- and *S*-wave velocity structure (depth to 800 km and expansion to 70 km) for each model (a–c) is shown.

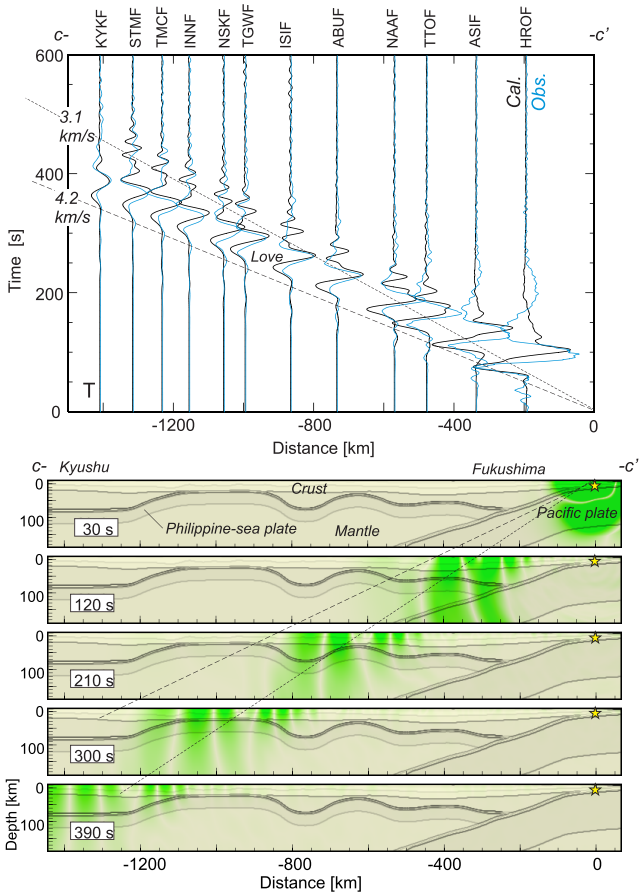

Figure 10. Synthetic record section of T-component ground displacement obtained from 3-D FDM simulation for the 2011 Off Tohoku earthquake as a function from CMT origin time, compared with the observed ground motion (blue traces) at the F-net station (see, Fig. 7 for locations). A bandpass filter between 0.005–1 Hz is applied to both observed and synthetic seismograms. The bottom panel shows the snapshots of T-component seismic wavefield at 30, 120, 210, 300 and 390 s from the CMT origin time in vertical profile of *c–c'* in Fig. 5. See also for Movie S2.

the complex source-rupture behaviour of the M_w 9.0 Off Tohoku earthquake (e.g. Lee *et al.* 2011; Yokota *et al.* 2011; Yoshida *et al.* 2011).

4 *G*-WAVE AT TELESEISMIC DISTANCES

Although the moderate-period (15–20 s) Love wave pulses attenuate with long-distance propagation across Japan, the longer-period (70 s) surface waves caused by the large, M_w 9.0 Off Tohoku earthquake were able to travel to teleseismic distances carrying a large amount of energy.

4.1 Ground motions from 2011 Off Tohoku earthquake

Fig. 11 shows a broad-band (0.003–1 Hz) teleseismic record of three-component displacement from the 2011 Off Tohoku earthquake at station SNZO in New Zealand at an epicentral distance of 9400 km. We see a distinctive long-period Love-wave pulse with a maximum ground motion of 8 mm on the T component with a dominant period of about 170 s (Fig. 11b).

Such long-period Love wave pulses observed with periods 40–500 s and nearly constant group velocity of about 4.4 km s^{-1} were first discovered by Gutenberg & Richter (1934). The pulse was later named the *G* wave in honour of Gutenberg. Sato (1958) evaluated the effect of the steep velocity gradient of the upper-mantle structure in generating nearly constant group velocity of the Love waves over a wide period band that generates the *G* wave. Since then the *G* waves have been analysed extensively to investigate the velocity structure of the Earth's interior. For example, the discovery of the low-velocity zone in the mantle lid at depths between 100–200 km (e.g. Press *et al.* 1958; Press 1959) was based on the properties of Love wave dispersion.

After the occurrence of large earthquakes, a sequence of *G* waves (G1, G2, . . . , Gn) circulate the earth every 2.5 hr (Fig. 11c), with a phase shift of 90° each time the antipole is traversed (Brune *et al.* 1961). These multiple *G* waves have been used to investigate source properties such as earthquake moment and stress drop etc. (e.g. Aki 1966a,b), and for examining *Q* structure of the upper mantle from the ratios of the Gn spectra (e.g. Kaminuma & Hirasawa 1964; Ben-Menahem 1965).

The similar sequence of Rayleigh waves is named R1, R2, . . . , Rn, and can be found on the R and Z components shown in Fig. 11(c). These arrivals are not as intense as the *G* waves due to the large dispersion of the Rayleigh waves compared with the Love waves on the T component.

4.2 *G* waves for oceanic and continental propagation

The efficiency of propagation of the *G* wave is recognized to be much stronger for oceanic than continental paths (Gutenberg & Richter 1934). This property is well demonstrated by comparison of broad-band record sections for ocean and continental stations at distances between 2000 and 10 000 km from the 2011 Off Tohoku earthquake (Fig. 12). The stations for the continental and oceanic paths are selected form the archive at the IRIS DMC for source-station azimuth ranges 127°–187° and –53° to 7° for which the radiation of the Love wave is enhanced.

The record section for oceanic paths (Fig. 12c) shows long-period *G*-wave pulses of about 170 s period propagating with large amplitudes at a speed of 4.4 km s^{-1}, followed by ripples with weakly dispersed short-period components less than 20 s. This efficient propagation of the long-period *G* waves is confirmed by 3-D FDM simulation of seismic wave propagation using the Parametric Earth Model (Dziewonski *et al.* 1975) for oceanic structure with a 7-km-thick crust (PEM-O; Fig. 12b), and a point double-couple source with a triangular 55 s time function (Fig. 12c-right-hand panel, also see S3 of Supporting Material for detail of the 3-D FDM simulation).

In contrast, the dispersion of the *G*-wave propagating through continental structure is very strong, with a long wave train that lasts over several hundred seconds (Fig. 12d). These properties of the dispersed *G* wave after travelling continental structure are clearly seen with 3-D FDM simulation using the PEM-C model of continental structure with a 35-km-thick crust (Fig. 12d-right-hand panel, also see Movie S4).

4.3 Dispersion curve

The large contrast between the character of the *G* wave pulses between the oceanic and continental environments is also manifest in the dispersion curves for Love waves in the PEM models (Fig. 13).

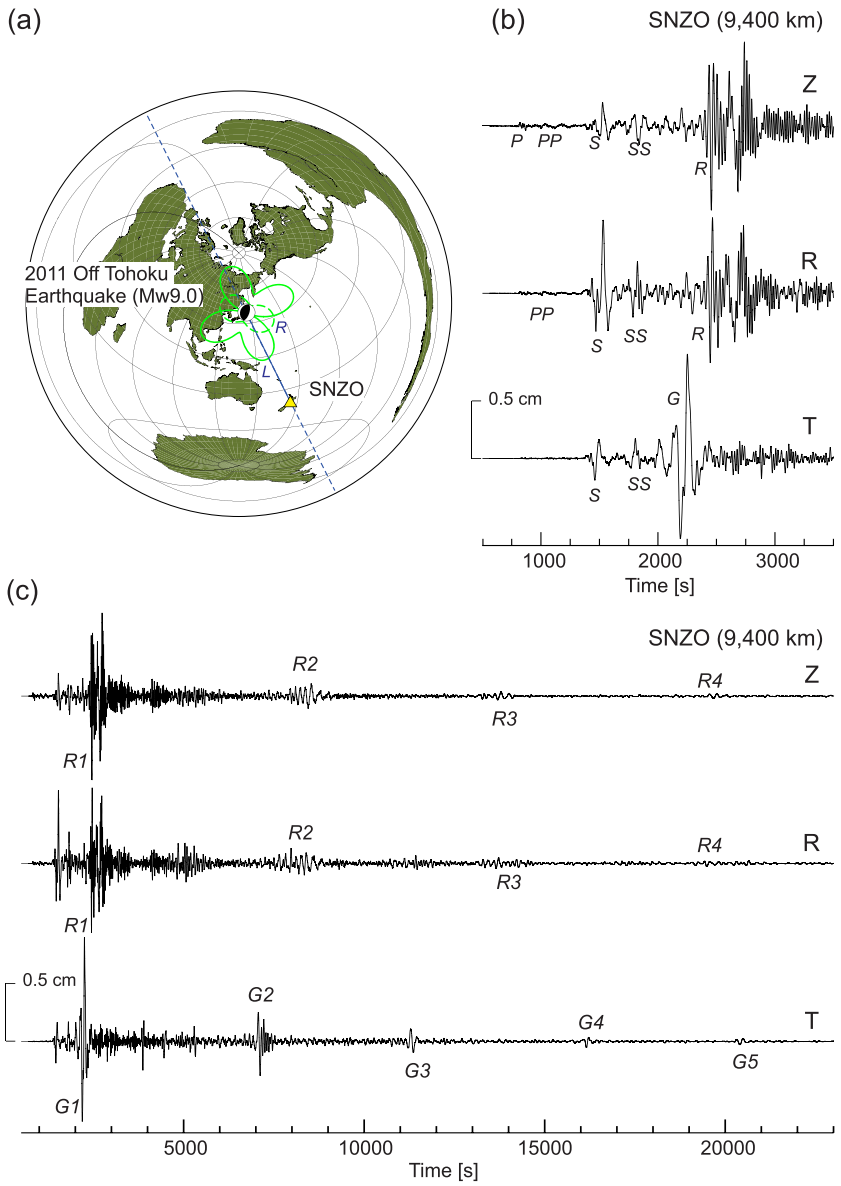

Figure 11. (a) Map showing the epicentre of the 2011 Off Tohoku, M_w 9.0 earthquake, station SNZO in New Zealand, and the radiation patterns of Rayleigh wave (dashed line) and Love wave (solid line). (b) Three-component broad-band (0.003–1 Hz) record of ground displacement at station SNZO at epicentral distance 9400 km and (c) long-duration record section with time axis expanded to 23 000 s showing multiple *G* waves after circling the Earth. Major phases are indicated.

Here, we show the dispersion curves in a slightly different format, with a horizontal axis representing slowness and vertical axis representing frequency, rather than the conventional frequency–velocity diagrams shown above. An advantage of this slowness-frequency diagram is that, after multiplying the epicentral distance by the slowness, the horizontal axis becomes the traveltime. Thus, it is easy to make comparisons with record sections and seismogram frequency–time plots.

Fig. 13(a) shows the theoretical dispersion curve of the Love-wave group velocity in the slowness-frequency domain calculated with the PEM-O model, superposed on the frequency–time plot of the T-component record of TAU in Tasmania, Australia after travelling 8917 km of the oceanic path. The theoretical dispersion curve of the Love wave for the oceanic PEM-O shows nearly constant group slowness of the fundamental-mode Love wave of 0.23 s km^{-1} (group velocity 4.3 km s^{-1}) over a wide period range from 11 to 270 s (Fig. 13a). This behaviour produces large-amplitude Love-wave pulse with a concentration of wide-period band of signals.

In addition, the phase velocity of the fundamental-mode Love wave in Fig. 13(a) has a value close to the group velocity, so that the *G*-wave propagates without change of pulse shape, as seen in the record section for oceanic stations (Fig. 12c). The theoretical dispersion curves also indicate that the overlap of higher-modes with group velocities similar to the fundamental mode over a wide period band further enhances the *G*-wave pulse. Such contributions of higher-modes to generating large *G*-wave pulses was also mentioned by Yoshida (1983) from calculations of waveforms of fundamental- and higher-modes of Love waves.

The frequency–time plot of the T-component record of KIEV in Kiev, Ukraine with 8298 km of travel on a continental path shown in Fig. 13(d) displays a large variation in slowness with increasing period from 25 to 80 s. The theoretical dispersion curve of the

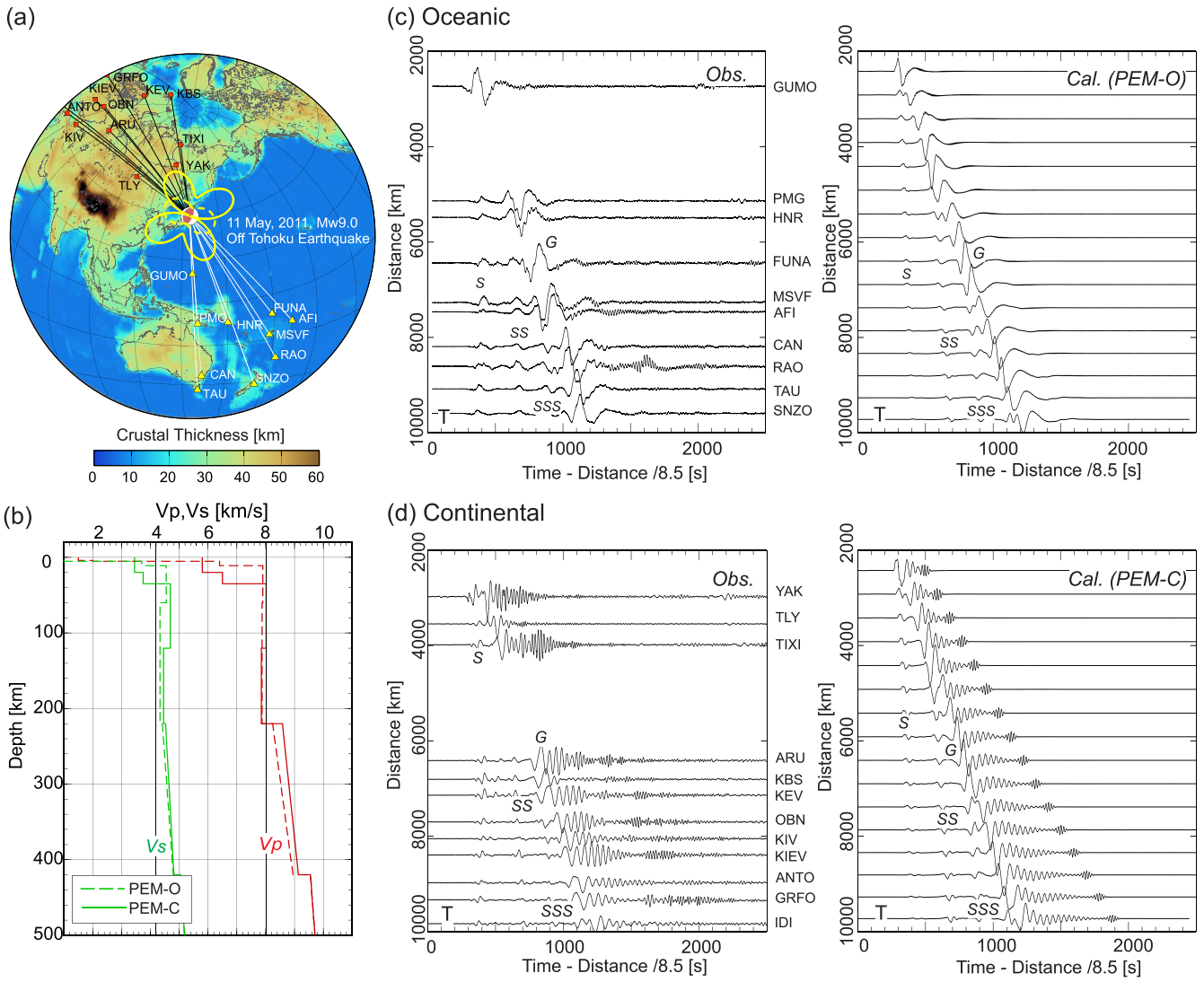

Figure 12. (a) Map showing the crustal thickness (after CRUST1.0; Laske *et al.* 2013) and ray paths from hypocentre of the 2011 Off Tohoku earthquake to IRIS GDSN stations. Radiation patterns of the Love wave (solid lines) and Rayleigh wave (dashed lines) are shown. (b) Velocity models PEM-C (continental structure) and PEM-O (oceanic structure) after Dziewonski *et al.* (1975). Broad-band record sections of T-component ground displacement for GDSN stations with propagation of surface waves along (c) oceanic paths (white lines on the map) and (d) continental paths (black lines), compared with the synthetic seismograms obtained by 3-D FDM simulations with the PEM-O and PEM-C models on the right. A band pass filter between 0.003 and 1 Hz is applied to both observed and synthetic seismograms.

fundamental-mode Love wave calculated for the continental structure PEM-C shown in Fig. 13(b) explains this strongly dispersed Love wave in the observed record and the frequency–time plot of the T-component record at station KIEV (Fig. 13b).

The theoretical dispersion curve of the continental PEM-C model with a nearly constant group velocity of about 4.5 km s^{-1} (slowness of 0.223 s km^{-1}) for the first and second higher modes for periods between 12 and 25 s indicates a possible G-type pulse. Such a higher-mode G-type wave is named the *Sa* wave, and is often observed in teleseismic records with period 10–30 s and a group velocity of 4.4–4.5 km s^{-1} (Brune 1965; Thatcher & Brune 1969). However, the amplitude of the *Sa* wave was too small to see in the T-component record section of the 2011 Off Tohoku earthquake at continental stations (Fig. 12d) and in the frequency–time plot of KIEV record (Fig. 13d). On the other hand, *Sa* phases from higher-mode Rayleigh waves are clearly observed on both the R and Z components (see section 4 of the Supporting Information).

5 DISCUSSION

The propagation of the large-amplitude Love-wave pulse from the 2016 Central Tottori, M_w 6.2 earthquake across western Japan not only caused impacts directly from strong ground motion, but also some unexpected effects such as overestimation of surface wave magnitude. Further, the propagation of long-period G waves from the destructive 2011 Off Tohoku, M_w 9.0 earthquake carried a large amount of seismic energy across the globe, triggering tremors and earthquakes immediately after the passage of these large-amplitude surface waves.

5.1 Magnitude overestimates by Love-wave pulses

The estimated magnitude of M_j 6.6 of the JMA of the 2016 Central Tottori earthquake was much larger than the moment magnitude M_w 6.2 of JMA, NIED, NIEC and the GCMT project. The value of

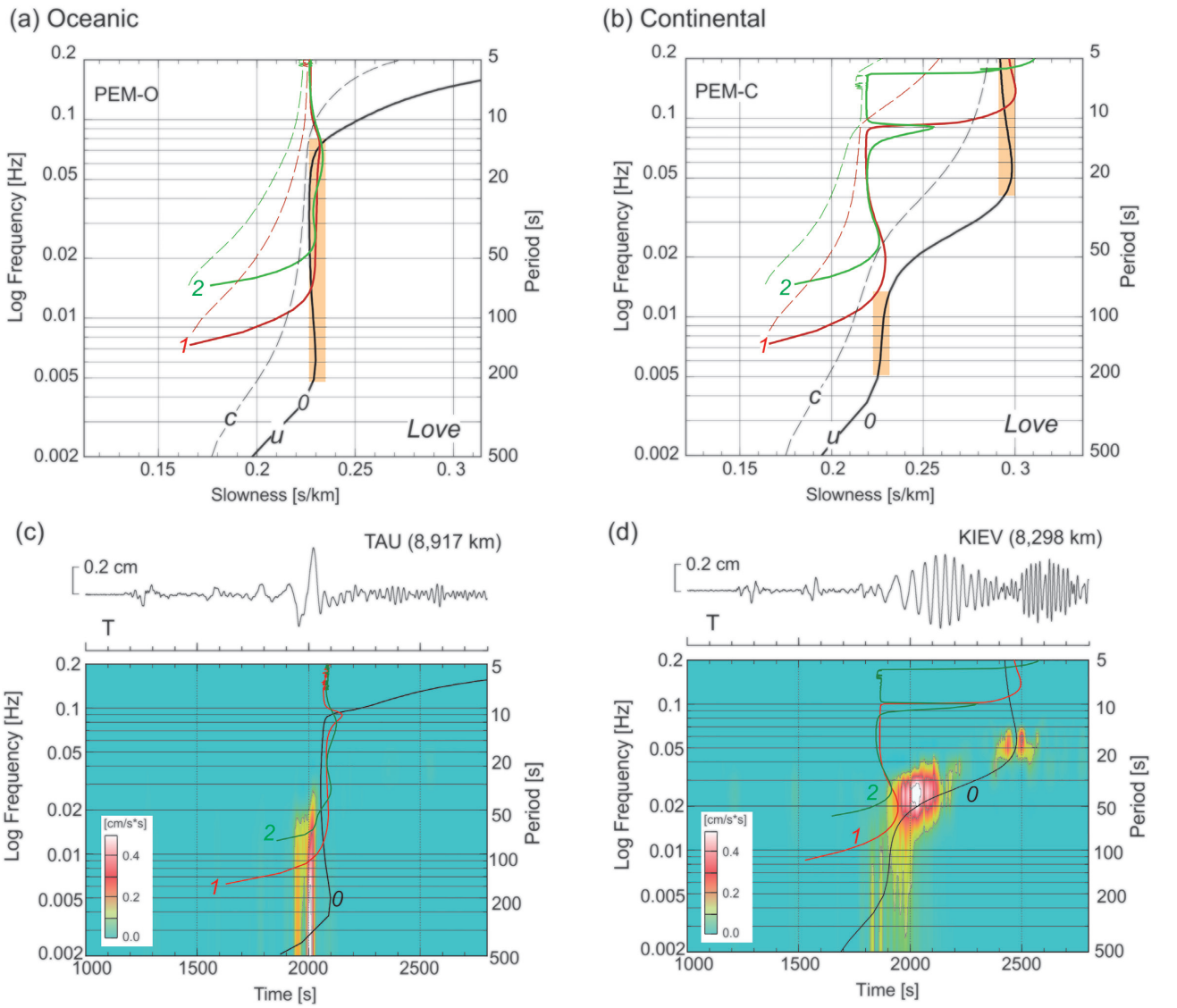

Figure 13. Theoretical Love-wave dispersion curves in frequency-slowness format, for (a) the phase (c) and group (u) slowness of the oceanic PEM-O model and (b) the continental PEM-C model (see, Fig.12b for velocity structure). The orange highlight indicates nearly flat group velocity that corresponds to a Love-wave pulse, (c) Frequency–time plot for the T-component ground displacement record at station TAU (distance is 8917 km) over the oceanic path, and at KIEV (8298 km) with a continental path. The Love-wave group slowness dispersion curves of fundamental (black) and first (red) and second (green) higher-modes are superimposed.

M_j tends to be larger than M_w in large shallow inland earthquakes (e.g. Takemura *et al*. 1990; Furumura and Kennett 2001; Dan *et al.* 2010), and the overestimate is particularly large in the earthquakes of western Japan including this 2016 Central Tottori earthquake (Kawamoto 2018). An overestimate of M_j for the 2000 Western Tottori earthquake (M_j 7.3 versus M_w 6.8), with a hypocentre close to the 2016 event, sparked considerable debate about the reasons for limited damage (0 dead, 182 injured, after Cabinet Office Disaster Prevention 2000) because M_j 7.3 was as large as the 1995 Kobe, Japan earthquake which occurred 5 yr before and killed 6400 people. Because the 2000 Western Tottori earthquake did not show any faults on the surface, the large M_j had a large influence on the consideration of the maximum magnitude of possible hidden faults below the surface in strong motion hazard assessment after this earthquake (e.g. Kagawa *et al.* 2005; Shimazaki 2008; Toda 2013).

The M_j value for shallow earthquakes (<60 km) is calculated based on the maximum amplitude of a displacement seismometer with a natural period of 6 s, with corrections for attenuation as a function of source–station distances based on Tsuboi (1954) with a revision by Katsumata (2004):

$$\mathrm{M}_{ka} = \log 10 A_d + \beta_{ka}(D, H),$$

where A_d is the maximum amplitude of ground displacement (in micrometre) and β_{ka} represents the attenuation function with parameters of epicentral distance D and focal depth H. First, M_{ka} is calculated for all observed seismic records, and then M_j is obtained by averaging M_{ka} over the span of epicentral distances of 30–700 km (Katsumata 2004).

The large overestimate of M_j for the 2016 Central Tottori and 2000 Western Tottori earthquakes can be explained as an effect of the propagation of large-amplitude Love-wave pulses in western Japan, as seen in the record section and PGD distributions shown in Fig. 1. From the K-NET and KiK-net records we calculated M_{ka} values (Fig. 14a). The M_{ka} estimates increase steadily with epicentral

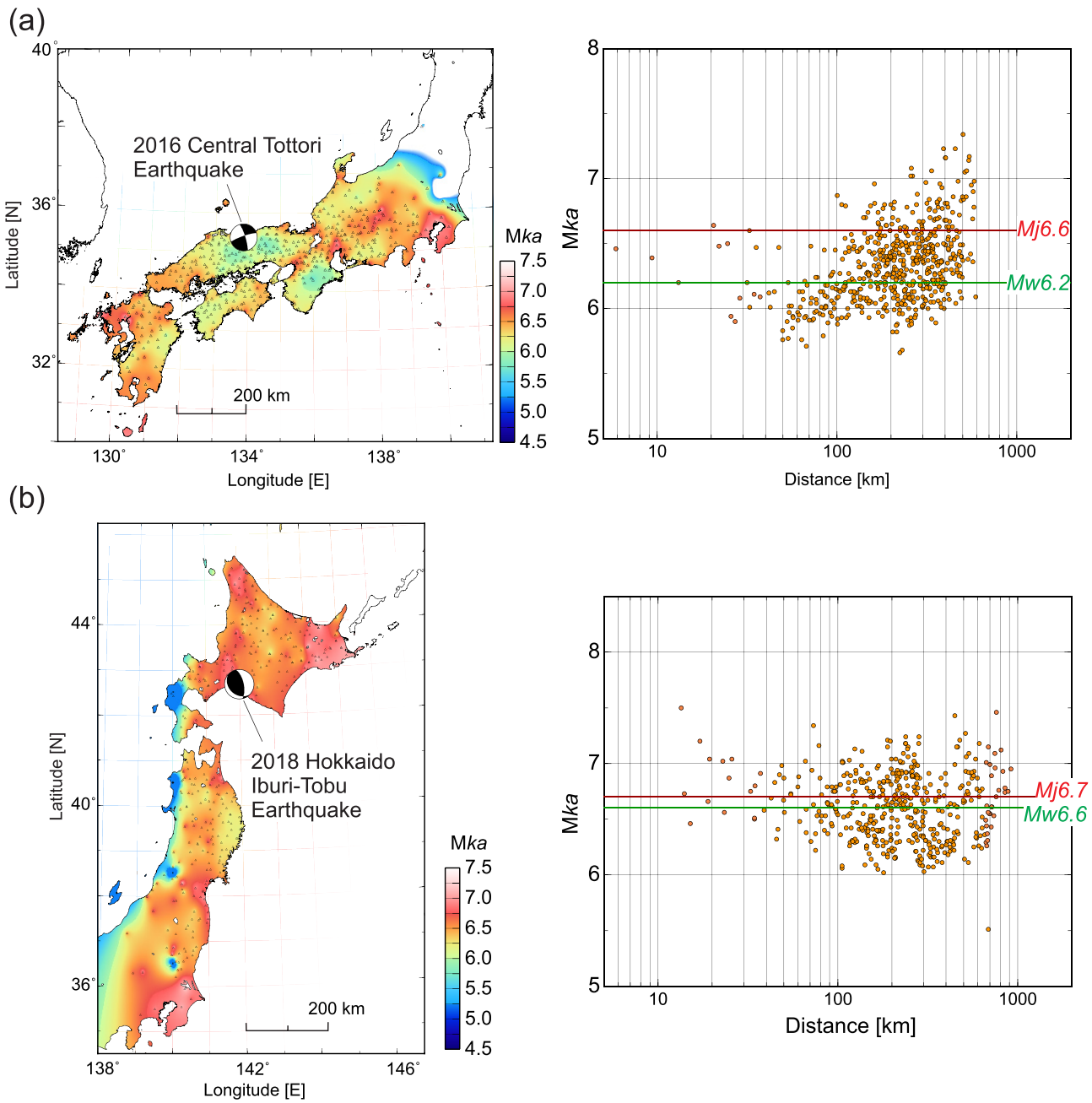

Figure 14. (a) Spatial distribution of estimated M_{ka} using the K-NET and KiK-net strong motion records for the 2016 Central Tottori earthquake. The right panel shows the distribution of M_{ka} as a function of epicentral distance. The estimated *M*j and *M*w values from JMA are also indicated. (b) Same as (a) but for the 2018 Hokkaido Iburi-Tobu earthquake.

distance, especially at distances over 100 km, so averaging of M_{ka} over the epicentral distance range from 30 to 700 km will produce large M_j estimates by JMA from the high M_{ka} at large distances. For such inland earthquakes in western Japan the presence of large-amplitude Love-wave pulse propagation means that M_j estimates should not use distant records. As can be seen from Fig. 14(a), no significant overestimate M_j will occur if the average of M_{ka} is taken for much shorter distances (e.g. 100–200 km).

For a reference, M_{ka} was also calculated using the K-net and KiK-net records of the Hokkaido Iburi-Tobu, Japan, M_w 6.6 (M_j 6.7) earthquake of 6 September 2018 at a depth of 37 km. The result shown in Fig. 14(b) shows that, although the deviations of the estimated M_{ka} are large due to large site effects, the averaged M_{ka} is almost constant regardless of epicentral distance and does not increase with distance. As we see from the record sections for the 2016 Central Tottori (Fig. 1) and 2011 Off Tohoku earthquakes (Fig. 5), the propagation of surface waves is not strong in northeastern Japan and in Hokkaido. Moreover, the relatively deeper source of this earthquake contributes to weaker surface waves.

5.2 Seismic triggering by Love-wave pulse

Many studies have reported that the 2011 Off Tohoku, M_w 9.0 earthquake increased seismicity of earthquakes and tremors in Japan

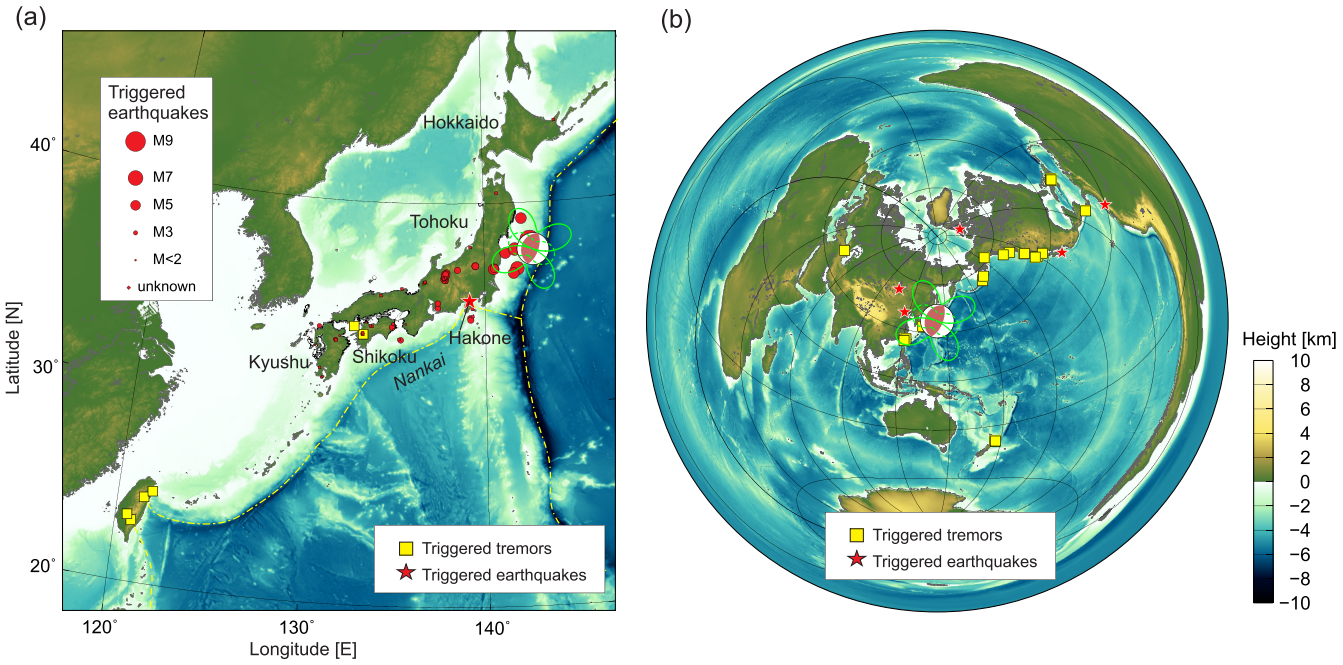

Figure 15. Summary maps of triggered earthquakes (red circles and stars) and tremors (yellow squares) locations due to the 2011 Off Tohoku earthquake. (a) Triggered earthquakes and tremors in the area around Japan after Miyazawa (2011), Chao *et al.* (2013), and Yukutake *et al.* (2013) and (b) over the globe after Gonzalez-Huizar *et al.* (2012) and Chao *et al.* (2013). The radiation pattern of Love (solid line) and Rayleigh waves (dashed line) are shown.

and over the globe (Fig. 15) as a result of the influence of large-amplitude and long-duration surface waves. For instance, Yukutake *et al.* (2013) reported that seismic activity beneath Hakone volcano in central Japan increased significantly with the passage of large-amplitude surface waves. Miyazawa (2011) discussed the triggering of seismic events in central to western Japan, but not in Tohoku and Hokkaido, due to the Off Tohoku earthquake. These authors explained that the dynamic stress change caused by the passage of large-amplitude surface waves is several orders of magnitude larger than the static stress change associated with the fault movement, and hence it can be the cause of the seismic wave triggering at larger epicentral distances. These studies did not examine the separate effects of Love and Rayleigh wave propagation. But, the large-amplitude Love-wave pulse observed in western Japan during the 2011 Off Tohoku earthquake as shown in Fig. 7 can be expected to have had a major impact on the stress change in the crust of central to western Japan and in the plate boundary of the subducting Philippine-sea Plate, rather than by the effect of weak but long-duration shaking from dispersed surface waves.

It has also been reported that the passage of surface waves from the 2011 Off Tohoku earthquake activated a sequence of low-frequency earthquakes (tremors) in Shikoku, western Japan (Chao *et al.* 2013) and in Taiwan (Gonzalez-Huizar *et al.* 2012; Chao *et al.* 2013) 1500 km away from the epicentre, which is also consistent with the stronger radiation pattern of Love wave and the propagation of large amplitude Love-wave pulses in these directions (Fig. 15a). Chao *et al.* (2013) reviewed the induced seismicity associated with this earthquake across the globe and examined the tremor triggering potential at each site by calculating the Coulomb failure criterion and time dependent stress change due the effect of the surface waves. The authors claimed that the observed triggering of tremors is likely to be initiated by the Love wave rather than Rayleigh wave, at least for the bursts of tremors in Nankai, Aleutian Arc, Alaska and Vancouver Island. Gonzalez-Huizar *et al.* (2012) searched the International Seismological Center (ISC) catalogue and broad-band records from the IRIS DMC, and detected microtremors and earthquakes in the records at stations in US, Russia, China, Ecuador and Mexico during the passage of the surface waves from the 2011 Off Tohoku earthquake. They also reported possible delayed triggering of large earthquakes a few days after the passage of large surface waves in Baja California and Mexico.

Fig. 15(b) shows the location of the activated tremors across the globe summarized by Chao *et al.* (2013) and the triggered earthquakes or tremors confirmed by Gonzalez-Huizar *et al.* (2012) associated with the passage of surface waves from the 2011 Off Tohoku earthquake. This figure shows that most of the event triggering due to the earthquake occurred on the opposite side of the Pacific Ocean except for three sites on the continent. Since the potential locations of tremors and earthquakes are limited to specific subduction zones and are not uniform, it is rather difficult to examine relative contribution of Love and Rayleigh waves on the remote triggering just by comparing with the radiation patterns of the surface waves. Nevertheless, large-amplitude *G*-wave pulse travelling across the Pacific Ocean as we saw in Fig. 12(c) and the successive Gn waves that circulate the earth many times can have large effects for activating seismicity on the opposite shore of the Pacific.

6 CONCLUSION

Usually, surface waves diminish in amplitude gradually with propagation, producing long wave trains due to dispersion. However, for crust without thick sediments and with a steep velocity gradient in the mantle the group velocity of the Love wave becomes nearly flat over a period bands from 10 to 20 s and 40 to 500 s generating large-amplitude Love-wave pulses (*G* wave) that travel long distances without significant dispersion.

The presence of thin low-velocity sediments with a strong contrast to basement in the continental crust allows the generation

and propagation of moderate-period (10–20 s) Love-wave pulses to regional distances. A similar phenomenon occurs between the low-velocity crust and the higher-velocity mantle with a steady *S*-wave velocity gradient with depth, develops longer-period (40–500 s) Love wave pulse (*G* wave) that travel to regional and teleseismic distances.

We have shown how such G-type Love-wave pulses can be generated with analyses of the observed strong ground motion records for the 2016 Central Tottori, Japan, M_w 6.2 earthquake and the 2011 Off Tohoku, Japan, M_w 9.0 earthquake, complemented by 3-D FDM simulation of seismic wave propagation in heterogeneous structure and construction of theoretical dispersion curves. The propagation of the longer-period *G* wave is more efficient when travelling across oceanic structure with a thinner crust, and maintains a distinct wave packet for long distances. Such large *G*-wave pulses can be a cause of sudden increase in seismic activity across the entire globe associated with large shallow earthquakes, for example the induction of tremors and earthquakes reported immediately after the occurrence of the 2011 Off Tohoku earthquake,.

ACKNOWLEDGEMENTS

We thank P. Kolínský and an anonymous reviewer, and the Editor Andrea Morelli for their careful reading and constructive comments that greatly improved the manuscript. The K-NET and KiK-net strong motion records and F-net broad-band records used in this study are available at the NIED Web page (http://www.mowlas.bosai.go.jp). The GDSN records are provided by the IRIS Data Management Centre (http://ds.iris.edu/ds/nodes/dmc/). The Japan Integrated Velocity Structural Model (JIVSM) is available at the Web page of the Headquarters for Earthquake Research Promotion, Japan. The FDM simulation is conducted using the OpenSWPC seismic wave propagation simulation code which is distributed at GitHub (https://github.com/takuto-maeda/OpenSWPC). Maps in the paper are drawn using the Generic Mapping Tools (Wessel & Smith 1998; http://gmt.soest.hawaii.edu/).

This study was conducted with support from Grants-in-Aid from the Japan Society for the Promotion of Sciences (Nos. 17K01322, 19H00807). The computations were conducted using the Earth Simulator at Japan Agency for Marine-Earth Science and Technology (JAMSTEC), and the Oakforest-PACS jointly operated at the Supercomputer Center of the University of Tokyo and the University of Tsukuba.

REFERENCES

Aki, K., 1966a. Generation and propagation of G waves from the Niigata earthquake of June 16, 1964, *Bull. Earthq. Res. Inst.,* **44,** 23–72.

Aki, K., 1966b. Generation and propagation of G waves from the niigata earthquake of June 16, 1964. Part 2. Estimation of earthquake moment, released energy, and stress-strain drop from the g wave spectrum, *Bull. Earthq. Res. Inst.,* **44,** 73–88.

Ben-Menahem, A., 1965. Observed attenuation and Q values of seismic surface waves in the upper mantle, *J. geophys. Res.,* **70**(18), 4641–4651.

Brune, J.N., Nafe, J.E. & Alsop, L.E., 1961. The polar phase shift of surface waves on a sphere, *Bull. seism. Soc. Am.,* **51,** 247–257.

Brune, J.N., 1965. The Sa phase from the Hindu Kush earthquake of July 6, *Pageoph,* **62,** 81–95.

Cabinet Office Disaster Prevention, 2000. About the Western Tottori Earthquake (summary), http://www.bousai.go.jp/updates/tottori/tottorigaiyo.html, in Japanese.

Chao, K.P., Zhigang, Gonzalez-Huizar, H., Aiken, C., Enescu, B., Kao, H., Velasco, A.A., Obara, K. & Matsuzawa, T., 2013. A global search for triggered tremor following the 2011 Mw 9.0 tohoku earthquake, *Bull. seism. Soc. Am.,* **103,** 1551–1571.

Dan, K., Muto, M., Ishii, Y. & Abiru, T., 2010. Relationships among different magnitudes for inland earthquakes classified by fault type and their application to strong motion prediction, *J. Strct, Constr. Eng, AIJ,* **75,** 741–750, in Japanese.

Dziewonski, A.M., Hales, A.L. & Lapwood, E.R., 1975. Parametrically simple earth models consistent with geophysical data, *Phys. Earth planet. Int.,* **10,** 12.

Furumura, T. & Kennett, B.L.N., 2001. Variations in regional phase propagation in the area around Japan, *Bull. seism. Soc. Am.,* **91,** 667–682.

Gonzalez-Huizar, H., Velasco, A.A., Peng, Z. & Castro, R., 2012. Remote triggered seismicity caused by the 2011, M 9.0 Tohoku, Japan earthquake, *Geophys. Res. Lett.,* **39,** L10302.

Gutenberg, B. & Richter, C.F., 1934. On seismic waves, *Getlands Beitr. z. Geophys.,* **43**.

Kagawa, T., Kazuo, D., Ohtsuka, Y. & Motohashi, S., 2005. A technique setting probability of buried rupture earthquake for probabilistic earthquake hazard estimation, *Proc. JSCE Earthquake Engineering Symposium,* **28,** https://doi.org/10.11532/proee2005a.28.47, in Japanese.

Kaminuma, K. & Hirasawa, T., 1964. The phase velocity of Love waves from an Iranian earthquake, *Zisin,* **17,** 139–147, in Japanese.

Katsumata, A., 2004. Revision of the JMA displacement magnitude, *Quart. J. Seismol.,* **67,** 1–10.

Kawamoto, H., 2018. Influence of regional characteristics of surface wave propagation characteristics on JMA magnitude estimates, *MSc thesis*, Department of Earth and Planetary Sciences, Faculty of Sciences, The University of Tokyo.

Kennett, B.L.N., Engdahl, E.R. & Buland, R., 1995. Constraints on seismic velocities in the Earth from travel times, *Geophys. J. Int.,* **122,** 108–124.

Koketsu, K., Miyake, H., Fujiwara, H. & Hashimoto, T., 2008. Progress towards a Japan integrated velocity structure model and long-period ground motion hazard map, in *Proceedings of the 14th World Conference on Earthquake Engineering,* pp. S10–038.

Laske, G., Masters, G., Ma, Z. & Pasyanos, M., 2013. Update on CRUST1.0—a 1-degree global model of Earth's crust, *Geophys. Res. Abstracts,* **15,** Abstract EGU2013-2658.

Lee, S.-J., Huang, B.-S., Ando, H., Chiu, H.-C. & Wang, J.-H., 2011. Evidence of large scale repeating slip during the 2011 Tohoku-Oki earthquake, *Geophys. Res. Lett.,* **38,** L19306, doi:10.1029/2011GL049580.

Maeda, T., Takemura, S. & Furumura, T., 2017. OpenSWPC: an open-source integrated parallel simulation code for modeling seismic wave propagation in 3D heterogeneous viscoelastic media, *Earth Planets Space,* **69,** 102.

Miyazawa, M., 2011. Propagation of an earthquake triggering front from the 2011 Tohoku-Oki earthquake, *Geophys. Res. Lett.* **38,** doi:10.1029/2011GL049795.

Montagner, J.P. & Kennett, B.L.N., 1996. How to reconcile body-wave and normal-mode reference Earth models? *Geophys. J. Int.,* **125,** 229–248.

National Research Institute for Earth Science and Disaster Resilience, 2019a. *NIED K-NET, KiK-net,* National Research Institute for Earth Science and Disaster Resilience, doi:10.17598/NIED.0005.

National Research Institute for Earth Science and Disaster Resilience, 2019b. *NIED F-net,* National Research Institute for Earth Science and Disaster Resilience, doi:10.17598/NIED.0004.

Noguchi, S., Maeda, T. & Furumura, T., 2017. The cause of long-time-duration long-period ground motion observed in Hokkaido during off-Tohoku earthquakes, in *JpGU-AGU Joint Meeting 2017,* Makuhari, May 2017, SSS08-P10.

Press, F., 1959. Some implications on mantle and crustal structure from G waves and Love waves, *J. geophys. Res.,* **1959,** 565–569.

Press, F., Ewing, M. & Lehner, F., 1958. A long-period seismograph system, *Trans. Am. Geophys. Un.,* **39,** 106–108.

Sato, Y., 1958. Attenuation, dispersion, and the wave guide of the G wave, *Bull. seism. Soc. Am.,* **48,** 231–251.

Shimazaki, K., 2008. Long-term forecast of large earthquakes on active faults in Japan: estimation of earthquake frequency, *Active Fault Res.,* **28,** 41–51, in Japanese.

Takemura, M., Ikeura, T. & Sato, R., 1990. Scaling relations for source parameters andmagnitude of earthquakes in the Izu Peninsula region, Japan, *Sci. Rep. Tohoku Univ.,* **32,** 77–89, in Japanese.

Thatcher, W. & Brune, J.N., 1969. Higher mode interference and observed anomalous apparent Love wave phase velocities, *J. geophys. Res.,* **74,** 6603–6611.

Toda, S., 2013. Current issues and prospective view to the next step for long-term crustal earthquake corecast in Japan, *Jour. Geol. Soc. Japan,* **119,** 105–123, in Japanese.

Tsuboi, C., 1954. Determination of the Gutenberg-Richter's magnitude of earthquakes occurring in and near Japan, *Zisin,* **7,** 185–193, in Japanese.

Yokota, Y., Koketsu, K., Fujii, Y., Satake, K., Sakai, S., Shinohara, M. & Kanazawa, T., 2011. Joint inversion of strong motion, teleseismic, geodetic, and tsunami datasets for the rupture process of the 2011 Tohoku earthquake, *Geophys. Res. Lett.,* **38,** L00G21, doi:10.1029/2011GL050098.

Yoshida, Y., Ueno, H., Muto, D. & Aoki, S. 2011. Source process of the 2011 off the Pacific coast of Tohoku Earthquake with the combination of teleseismic and strong motion data, *Earth Planets Space,* **63,** 565–569.

Yoshida, M., 1983. Higher mode interference on oceanic Love waves excited by shallow earthquakes as inferred through synthetic waves, *Bull. Earthq. Res. Inst.,* **58,** 1–24.

Yukutake, Y., Honda, R., Harada, M., Ito, H., Minoru, S., Koketsu, K. & Akio, Y., 2013, Remotely-triggered seismicity in the Hakone volcano following the 2011 off the Pacific coast of Tohoku Earthquake, *Earth Planet Space,* **63,** https://doi.org/10.5047/eps.2011.05.004.

SUPPORTING INFORMATION

Supplementary data are available at *GJI* online.

Movies.zip

Figure S1. Peak ground displacement (PGD) from K-NET and KiK-net strong motion records (triangle marks), with focal mechanisms from the F-net of NIED, together with records of ground displacement [vertical (Z), radial (R) and transverse (T) component] obtained from F-net broad-band stations (green squares in the PGD map). A bandpass filter is applied for the band 0.01–1 Hz. (a) Western Tottori earthquake of 6 October 2000 (M_w 6.8), (b) Western Fukuoka earthquake of 26 March 2015 (M_w 6.7) and (c) the Kumamoto earthquake of 16 April 2016 (M_w 7.0).

Figure S2. (a) Map showing the location of foreshock (10 March 2011; M_w 6.0) and main shock (11 March 2011; M_w 9.0) of 2011 Off Tohoku, Japan earthquake. Record section of (b) T- and (c) R-component ground displacement obtained for F-net stations (blue squares) towards Kyushu (*a–a'*) and towards Hokkaido (*b–b'*) for the foreshock (M_w 6.0) of 2011 Off Tohoku earthquake. A bandpass filter is applied for the band 0.01–1 Hz. The group velocities of 4.2 and 3.1 km s^{-1} are indicated.

Figure S3. Snapshots of seismic wave propagation from the 3-D FDM simulation along a vertical cross-section at 240, 600, 960, 1320 and 1680 s after earthquake origin time. Synthetic record sections of T component ground displacement obtained using (a) the oceanic PEM-O model and (b) the continental PEM-C model. A bandpass filter is applied for the band 0.003–1 Hz. The star indicates the hypocentre of the earthquake. Major phases are marked on the snapshots and record section. See also Movies S3 and S4.

Figure S4. Theoretical dispersion curves of group (*u*; slid lines) and phase (*c*; dashed lines) velocities as a slowness-frequency plot for fundamental (black) and first (red) and second (green) higher-mode Rayleigh waves: (a) oceanic PEM-O and (b) continental PEM-C modes. Record section of vertical (Z) component ground displacement for the 2011 Off Tohoku earthquake recorded at (c) oceanic stations and (d) continental stations (see Fig. 12a for station locations). A bandpass filter is applied for the band 0.003–1 Hz. The group velocity of *Sa* (4.2 km s^{-1}) and fundamental-mode Rayleigh wave (3.8 km s^{-1}) are marked.

Please note: Oxford University Press is not responsible for the content or functionality of any supporting materials supplied by the authors. Any queries (other than missing material) should be directed to the corresponding author for the paper.